AD-A238 718

REPORT DOCUMENTATION PAGE

Form Approved
OMB No. 0704-0188

...ion is estimated to average 1 hour per response, including the time for reviewing instructions, searching existing data sources, ...ering and reviewing the collection of information. Send comments regarding this burden estimate or any other aspect of this ...ducing this burden, to Washington Headquarters Services, Directorate for Information Operations and Reports, 1215 Jefferson ...and to the Office of Management and Budget, Paperwork Reduction Project (0704-0188), Washington, DC 20503.

2. REPORT DATE: 25 Jun 1991

3. REPORT TYPE AND DATES COVERED: Final Report/15 Nov 88-14 Nov 90

4. TITLE AND SUBTITLE: Investigation of High Efficiency Monolithic Multibandgap Solar Cells

5. FUNDING NUMBERS: 61102F/2301/A7

6. AUTHOR(S):

Lawrence Olsen

7. PERFORMING ORGANIZATION NAME(S) AND ADDRESS(ES):

University of Washington
(WSU Tri-Cities)
100 Sprout Road
Richland WA 99352

8. PERFORMING ORGANIZATION REPORT NUMBER: AFOSR-TR- 91-0653

9. SPONSORING/MONITORING AGENCY NAME(S) AND ADDRESS(ES):
AFOSR/NP B1C 410
Bolling AFB DC 20332-6448

10. SPONSORING/MONITORING AGENCY REPORT NUMBER: AFOSR-89-0182

11. SUPPLEMENTARY NOTES

12a. DISTRIBUTION/AVAILABILITY STATEMENT: Approved for public release; distribution is unlimited.

12b. DISTRIBUTION CODE

13. ABSTRACT *(Maximum 200 words)*

This program concerned investigations of multibandgap solar cell structures with potential efficiencies greater than 40%. The basic concept utilized a monolithic stack of three or more cells based on AlGaAs and InGaAs ternary compounds. In particular, the planned work for the two year program was to involve research related to a three cell stack comprised of a top Al(.37)Ga(.63)As cell, a middle GaAs cell and a bottom In(.3)Ga(.7)As cell. Efforts first concentrated on GaAs cell growth and fabrication, and then on AlGaAs film growth. Although significant progress was made in the development of AlGaAs film growth, efforts to grow InGaAs films and solar cells were not initiated. GaAs solar cells were fabricated from epi-wafers grown at WSU Tri-Cities. The cells had a p/n structure with Au metallization and SiO anti-reflection coatings. Cells exhibited AM1.5 efficiencies greater than 21%. Studies of AlGaAs included development of procedures for growth of films of known aluminum concentration and measurement of minority carrier properties. The minority carrier diffusion length was found to be 0.6 um for AlGaAs with a composition corresponding to 10% aluminum. Films with larger amounts of Al exhibited much lower values of diffusion length. Studies were conducted which determined that oxygen impurity levels in the AlGaAs were degrading minority carrier properties.

14. SUBJECT TERMS

15. NUMBER OF PAGES: 42

16. PRICE CODE

17. SECURITY CLASSIFICATION OF REPORT	18. SECURITY CLASSIFICATION OF THIS PAGE	19. SECURITY CLASSIFICATION OF ABSTRACT	20. LIMITATION OF ABSTRACT
UNCLASSIFIED	UNCLASSIFIED	UNCLASSIFIED	UL SAR

INVESTIGATION OF HIGH EFFICIENCY MONOLITHIC

MULTIBANDGAP SOLAR CELLS

FINAL REPORT

For Period

11/15/88 - 11/11/90

A-1

AFOSR GRANT: AFOSR - 89 - 0182
START DATE: 11/15/88
CONTRACTOR: UNIVERSITY OF WASHINGTON
(WSU TRI-CITIES)
PRINCIPAL INVESTIGATOR: Dr. Larry C. Olsen

91-05913

ABSTRACT

This program concerned investigations of multibandgap solar cell structures with potential efficiencies greater than 40%. The basic concept utilized a monolithic stack of three or more cells based on AlGaAs and InGaAs ternary compounds. In particular, the planned work for the two-year program was to involve research related to a three-cell stack comprised of a top $Al_{.37}Ga_{.63}As$ cell, a middle GaAs cell and a bottom $In_{.3}Ga_{.7}As$ cell. Efforts first concentrated on GaAs cell growth and fabrication, and then on AlGaAs film growth. Although significant progress was made in the development of AlGaAs film growth, efforts to grow InGaAs films and solar cells were not initiated. GaAs solar cells were fabricated from epi-wafers grown at WSU Tri-Cities. The cells had a p/n structure with Au metallization and SiO anti-reflection coatings. Cells exhibited AM1.5 efficiencies greater than 21%. Studies of AlGaAs included development of procedures for growth of films of known aluminum concentration and measurement of minority carrier properties. The minority carrier diffusion length was found to be 0.6 μm for AlGaAs with a composition corresponding to 10% aluminum. Films with larger amounts of Al exhibited much lower values of diffusion length. Studies were conducted which determined that oxygen impurity levels in the AlGaAs were degrading minority carrier properties.

TABLE OF CONTENTS

1. INTRODUCTION 1
   1.1 Research Objectives 1
   1.2 Technical Approach 1
   1.3 Benefits of AFOSR Funding 1
2. MOCVD GROWTH OF GaAs 3
   2.1 MOCVD System at WSU Tri-Cities 3
   2.2 Carrier Mobility in Undoped GaAs 3
   2.3 Growth of N- and P-Type GaAs 3
3. MOCVD GROWTH OF $Al_xGa_{1-x}As$ FILMS 6
   3.1 Growth of AlxGa1-xAs Films 6
   3.2 Aluminum Composition by X-ray Analysis 7
   3.3 Majority Carrier Concentration Determination 9
4. MINORITY CARRIER DIFFUSION LENGTH OF $Al_xGa_{1-x}As$ FILMS 12
   4.1 Schottky Barrier Photoresponse 12
   4.2 Fabrication of Schottky Barriers 15
   4.3 Photoresponse Measurement 15
   4.4 Diffusion Length in AlxGa1-xAs Films 17
   4.5 Discussion of Results for AlGaAs Films 26
      4.5.1 Necessity of Dead Layer in Modeling Calculations 26
      4.5.2 Evidence Supporting Oxygen Contamination 27
5. EFFECT OF EUTECTIC METAL BUBBLER ON $Al_xGa_{1-x}As$ QUALITY 30
   5.1 Operation of Bubbler 30
   5.2 Effect on Minority Carrier Diffusion Length 31
6. GaAs SOLAR CELL GROWTH AND FABRICATION 34
   6.1 Epi-Layer Structure 34
   6.2 P/N Solar Cell Fabrication and Characterization 34

REFERENCES 37

APPENDIX A 38

APPENDIX B 39

APPENDIX C 40

LIST OF FIGURES

Figure 1. Carrier Mobility Versus Film Thickness for Undoped GaAs Films. 4
Figure 2. Electron Carrier Concentration Versus Silane Flow Rate for MOCVD GaAs Films Grown at 720 °C. 4
Figure 3. Hole Concentration Versus Film Growth Temperature for Two Flow Rates for DMZn. 5
Figure 4. Mole fraction AlAs vs. flow of TMAl for WSU Tri-Cities MOCVD reactor. 8
Figure 5. Shown are (a) a Schottky barrier device being measured for I_{sc} with photon flux $F_{h\nu}$ and (b) the associated band diagram. 14
Figure 6. Internal photoresponse versus wavelength for specimen A0-02-07 20
Figure 7. Internal photoresponse versus wavelength for specimen B0-02-07 20
Figure 9. Internal photoresponse versus wavelength for specimen A0-05-01 21
Figure 10. Internal photoresponse versus wavelength for a n-type GaAs specimen (A0-05-02). 22
Figure 11. Internal photoresponse versus wavelength for specimen A0-05-03 22
Figure 12. Internal photoresponse versus wavelength for specimen A0-05-15 23
Figure 13. Internal photoresponse versus wavelength for specimen A0-05-31 23
Figure 14. Internal photoresponse versus wavelength for specimen A0-06-01 24
Figure 15. Internal photoresponse versus wavelength for specimen B0-06-01 24
Figure 16. Internal photoresponse versus wavelength for specimen A0-06-04 25
Figure 17. Internal photoresponse versus wavelength for specimen A0-06-05 25
Figure 18. Shown above are (a) the physical representation of the Schottky barrier device including the dead layer, and (b) the corresponding band diagram 28
Figure 19. Internal photoresponse versus wavelength for x = 0.10 (p-type) specimens. 31

Figure 20. Layered Structure of GaAs Solar Cell Grown and Processed at WSU Tri-Cities 35
Figure 21. Illuminated I-V Characteristics of WSU Tri-Cities Cell Coupled to Approximate AM1.5 Illumination 35
Figure 22. Internal Photoresponse for High Efficiency GaAs Cell 36
Figure C-1. Spire 500XT MOCVD System Installed in the Electronic Materials Laboratory, WSU Tri-Cities 42

LIST OF TABLES

Table 3-1. Growth parameters of AlxGa1-xAs films 6
Table 3-2. Summary of majority carrier measurements 10
Table 4-1. Summary of photoresponse modeling results 28

1. INTRODUCTION

1.1 Research Objectives

This program concerned investigations of multibandgap solar cell structures with potential efficiencies greater than 40%. The basic concept utilized a monolithic stack of three or more cells based on AlGaAs and InGaAs ternary compounds. In particular, the planned work for the two-year program was to involve research related to a three-cell stack comprised of a top $Al_{.37}Ga_{.63}As$ cell, a middle GaAs cell and a bottom $In_{.3}Ga_{.7}As$ cell. Efforts first concentrated on GaAs cell growth and fabrication, and then on AlGaAs film growth. Although significant progress was made in the development of AlGaAs film growth, efforts to grow InGaAs films and solar cells were not initiated.

1.2 Technical Approach

The basic approach has involved growing III-V film structures with the SPIRE 500XT MOCVD reactor housed at WSU Tri-Cities, and which was purchased with a DoD university equipment grant in 1988. At the beginning of this program, the WSU MOCVD reactor was operational, but not yet calibrated. Thus, a significant part of the first-year effort concentrated on determining growth rate for GaAs, and approaches to doping GaAs. Epitaxial layered structures appropriate for GaAs solar cells were grown with the WSU reactor, and diced to provide die for cell fabrication. After processes for GaAs cell fabrication had been developed, work concerning AlGaAs film growth and cell fabrication began. MOCVD growth of GaAs and AlGaAs are discussed in Sections 2 and 3. Studies of minority carrier properties of AlGaAs films are presented in Section 4. Finally, GaAs solar cell fabrication and characterization are discussed in Section 5.

1.3 Benefits of AFOSR Funding

The funding provided during this two-year project has allowed the electronic materials program at WSU Tri-Cities to mature to the point that work presently being conducted on solar cells and transistors based on GaAs

and AlGaAs can be considered "forefront" research activities. Programs in heterojunction bipolar transistors and GAAs solar cells for space applications are being carried out by Dr. Olsen's group.

Contributors to this AFOSR program are listed in Appendix A; a list of publications generated as a result of this work are given in Appendix B.

2. MOCVD GROWTH OF GaAs

2.1 MOCVD System at WSU Tri-Cities

The Spire 500XT metalorganic chemical vapor deposition system was purchased in 1988 with a \$260,000 grant from the Department of Defense. The equipment was delivered in July, 1988 and installed in September, 1988. Initial operation occurred in October, 1988. Thus, it was necessary to calibrate the system during the early part of this effort. In particular, procedures were developed for growing high quality undoped GaAs, n-type and p-type GaAs, undoped AlGaAs and doped AlGaAs. The WSU MOCVD reactor is discussed in more detail in Appendix C.

2.2 Carrier Mobility in Undoped GaAs

Hall mobility is plotted versus film thickness in Figure 1 for undoped GaAs films grown in the WSU reactor. As shown, films have been grown that exhibit mobilities at 77 °K on the order of 80,000 $cm^2 Volt^{-1} sec^{-1}$. The films were grown at 650 °C, with a V-III ratio > 50 and at a pressure of 100 torr. As noted, the results compare favorably with other published data. The background dopant concentration was typically in the 10^{14} cm^{-3} range. The undoped films are always n-type due to unintentional Si doping.

2.3 Growth of N- and P-Type GaAs

Procedures were developed for doping GaAs n-type and p-type. N-type and p-type doping are achieved with substitutional dopants Si and Zn. These dopants are added as GaAs is being grown by mixing silane or dimethylzinc (DMZn) with trimethylgallium (TMGa) and arsine. More data have been accumulated for n-type doping because of the need to vary the doping in the n-type base of a P/N cell structure. Figure 2 shows results for n-type films grown at 720 °C. The electron concentration is plotted versus silane flow rate. Values of electron concentration were measured using a Hall effect measurement.

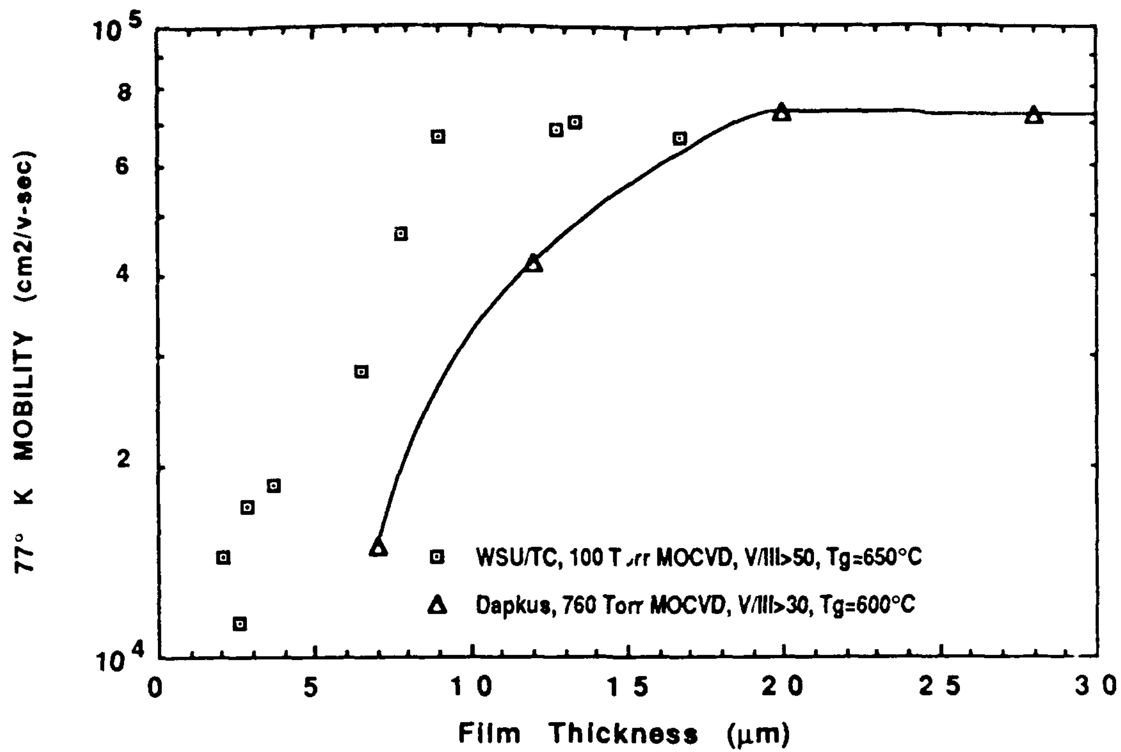

Figure 1. Carrier Mobility Versus Film Thickness for Undoped GaAs Films. Results Published by Dapkus Are Shown For Comparison.

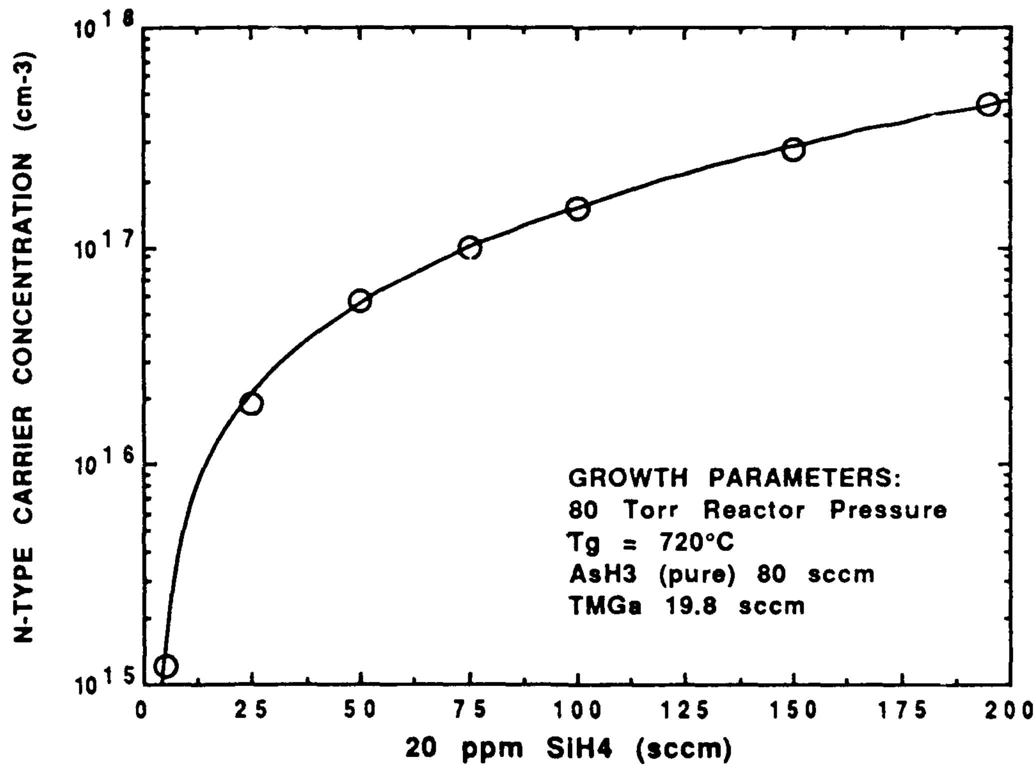

Figure 2. Electron Carrier Concentration Versus Silane Flow Rate for MOCVD GaAs Films Grown at 720 °C.

Data for the hole concentration in p-type films is plotted versus growth temperature in Figure 3. Results are shown for two values of DMZn flow rate. Less data has been acquired for p-type films since our interest for solar cells has involved emitter layers with the hole concentration on the order of 10^{18} cm^{-3} to 10^{19} cm^{-3}.

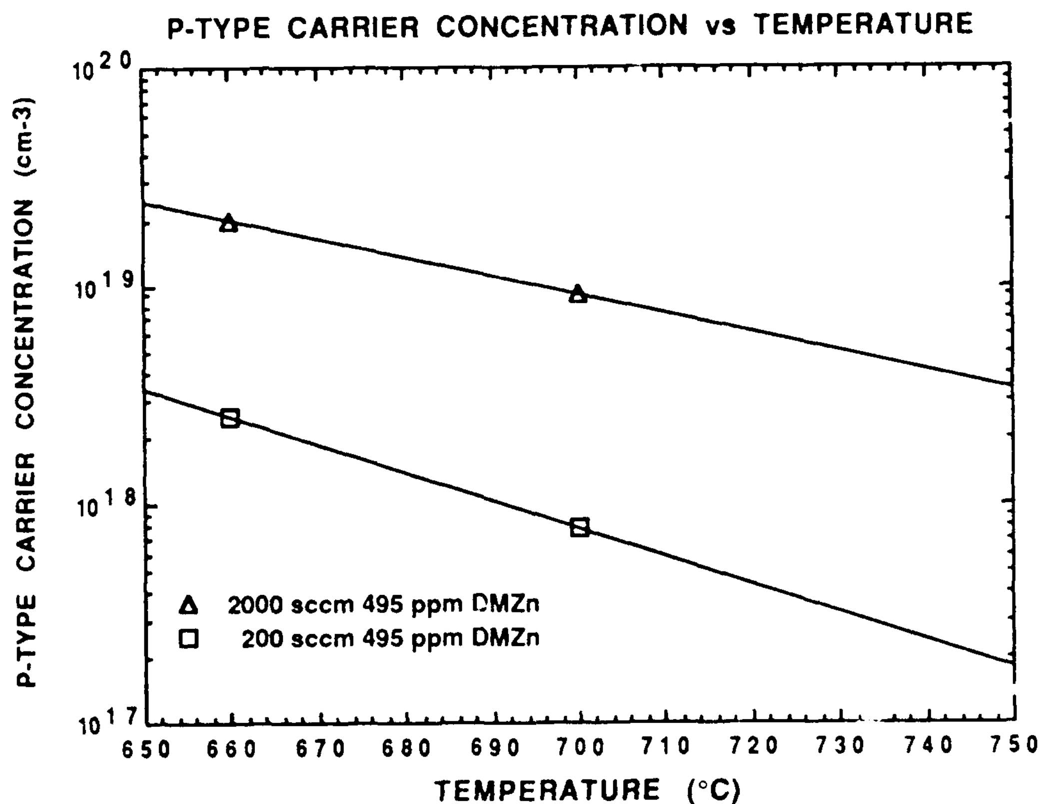

Figure 3. Hole Concentration Versus Film Growth Temperature for Two Flow Rates for DMZn.

3. MOCVD GROWTH OF $Al_xGa_{1-x}As$ FILMS

This section will first discuss how the growth of the films for this study was accomplished and will include a tabular summary of the growth parameters of all specimens. It will then discuss the determination of the composition of the $Al_xGa_{1-x}As$ films through x-ray diffraction and provide a figure comparing these experimental values to theoretical calculations. Finally, the two methods used to determine majority carrier concentration of films are discussed and a tabular summary of these results is provided.

3.1 Growth of $Al_xGa_{1-x}As$ Films

Trimethylgallium (TMGa) and trimethylaluminum (TMAl) were used as metalorganic sources for all of the film growths and pure AsH_3 served as the As source. Silane was used as the n-type dopant gas and dimethylzinc as the p-type dopant source. Palladium-diffused H_2 flowing at a total of 9 liters/min was used as the carrier gas for all precursors. The $Al_xGa_{1-x}As$ films were grown on conductive <100> GaAs substrates misoriented 2° towards <110>. Once the substrate was loaded into the reactor it was heated to the growth temperature and kept under a flowing AsH_3/H_2 ambient for 15 minutes prior to growth to deoxidize the GaAs surface. The metalorganic sources were then introduced into the reactor and the epitaxial film was grown at a typical rate of 12 Å/sec to a thickness of approximately 4 µm. The V/III ratio was maintained at a value of 49 for all growths and the reactor pressure was 80 torr.

Table 1 provides a summary of growth parameters for specimens grown for this study that includes the intended composition, growth temperature, and dopant flow rate. Several items are worth noting in the table. The first is the change in the growth temperature from 720 to 780 °C beginning with specimen A0-05-30. The increase was necessitated by the poor quality of the AlGaAs films grown up to this point in the study, and it was hoped that the minority carrier diffusion length would show significant improvement as a result. The second item to note is the dopant flow rate. Initially, the flow rates were chosen such that a consistent dopant concentration was achieved throughout the composition range studied, however, it was later decided to grow with a consistent flow rate of DMZn for

all p-type films to facilitate a measurement of the incorporation of Zn as a function of composition. The last item to note from Table 1 is whether or not the eutectic bubbler was in operation during the growth of the film. Initially, the bubbler was inactive and was not activated until the growth of specimen A0-05-31. The bubbler was activated in an effort to improve material quality by reducing the concentration of oxygenated impurities reaching the growth ambient via the arsine source gas.

Table 1. Growth parameters of $Al_xGa_{1-x}As$ films.

SPECIMEN	T_g °C	DOPANT FLOW	INTENDED COMPOSITION	EUTECTIC BUBBLER
A0-02-07	720	DMZn 300 sccm	$Al_{.3}Ga_{.7}As$	NO
B0-02-07	720	SiH_4 40 sccm	$Al_{.1}Ga_{.9}As$	NO
A0-02-13	720	SiH_4 40 sccm	$Al_{.2}Ga_{.8}As$	NO
A0-05-01	720	DMZn 200 sccm	$Al_{.1}Ga_{.9}As$	NO
A0-05-02	720	SiH_4 30 sccm	GaAs	NO
A0-05-03	720	DMZn 120 sccm	$Al_{.1}Ga_{.9}As$	NO
A0-05-15	720	DMZn 120 sccm	$Al_{.1}Ga_{.9}As$	NO
A0-05-30	780	DMZn 120 sccm	$Al_{.5}Ga_{.5}As$	NO
A0-05-31	780	DMZn 120 sccm	$Al_{.1}Ga_{.9}As$	YES
A0-06-01	780	DMZn 120 sccm	$Al_{.2}Ga_{.8}As$	YES
B0-06-01	780	DMZn 120 sccm	$Al_{.2}Ga_{.8}As$	YES
A0-06-04	780	DMZn 120 sccm	$Al_{.1}Ga_{.9}As$	YES
A0-06-05	780	DMZn 120 sccm	$Al_{.1}Ga_{.9}As$	YES
A0-07-11	780	DMZn 120 sccm	$Al_{.4}Ga_{.6}As$	YES
B0-07-11*	780	DMZn 120 sccm	$Al_{.6}Ga_{.4}As$	YES
A0-07-10*	780	DMZn 120 sccm	$Al_{.5}Ga_{.5}As$	YES
A0-07-12*	780	DMZn 120 sccm	$Al_{.1}Ga_{.9}As$	YES

* for x-ray analysis only

3.2 Aluminum Composition by X-ray Analysis

X-ray analysis was used to determine composition of AlGaAs films. Dr. Tom Roth of TRW, Inc. carried out the x-ray analysis. Data from TRW

included plots of countrate (intensity) versus seconds. The difference in the Bragg angles between the AlGaAs layer and the GaAs substrate is determined by measuring the distance between the two peaks on the plots, in inches, and then converting through the constant 50 arc sec/inch. Since the Bragg angle of the GaAs is known for the wavelength of radiation used, the Bragg angle of the AlGaAs can be determined which leads to the interplaner spacing of the 004 plane (since this is the reflecting plane of the analyzing crystal). Using the interplaner spacing, the composition of the AlGaAs was determined. A total of ten specimens (seven different compositions) were sent for x-ray analysis to determine composition.A plot of percentage AlAs versus TMAl flow as determined by x-ray analysis is shown in Figure 4. Shown for comparison is a line representing the theoretical compositions based on the partial pressures of the source precursors. There are several assumptions used in the theoretical calculations including a total reactor pressure of 80 torr, an excess of AsH_3 (V/III ratio > 1) in the growth ambient, a Group III total pressure of 0.0222 torr, TMGa and TMAl being held at 0 °C and 20 °C (700 torr), respectively, prior to entry into the reactor, and TMAl existing as a dimer in

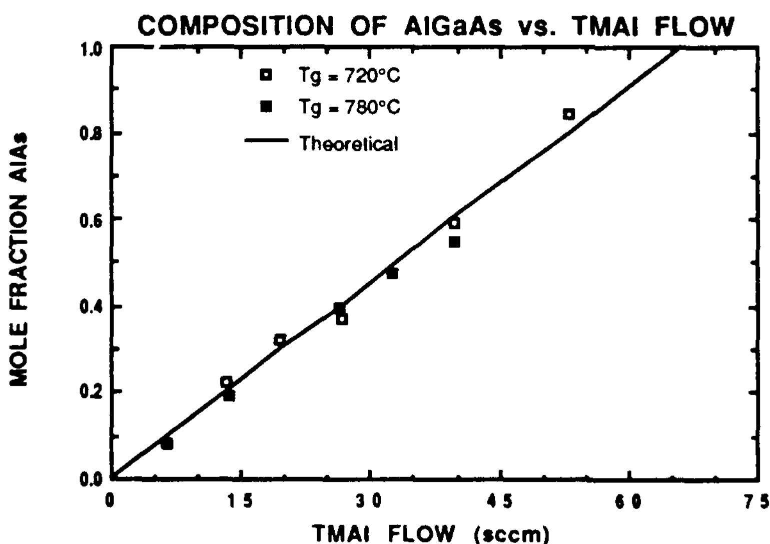

Figure 4. Mole fraction AlAs vs. flow of TMAl for WSU Tri-Cities MOCVD reactor. The squares represent data obtained by x-ray analysis and the solid line represents theoretical calculations. The following assumptions were used for the calculations: 80 torr total reactor pressure; Excess AsH_3; Group III pressure = 0.0222 torr; TMGa @ 0 °C and 700 torr; TMAl @ 20 °C and 700 torr; $Flow_{Ga}$ = 19.9 - $0.3Flow_{Al}$; TMAl exists as a dimer in the vapor phase.

the vapor phase. Note the generally good agreement between the experimental values and the theoretical calculations over the entire composition range.

3.3 Majority Carrier Concentration Determination

The measurement of the majority carrier concentration in AlGaAs films was accomplished by capacitance-voltage (C-V) analysis using small Al Schottky barriers and also using a Polaron electrochemical semiconductor profiler (the Polaron was also used to determine the thickness of the epitaxial layers). As discussed previously, by applying the parallel plate expression for capacitance to the Schottky barrier diode, the capacitance (C) of the depletion region can be approximated using the depletion region thickness (W). The depletion region thickness is related to the applied voltage (V_a) and the dopant concentration (N_D) allowing the net impurity concentration, N(x), as a function of epth to be derived resulting in the following equation:

$$N(x) = \frac{-C^3}{q e_r e_o A^2} \left[\frac{dC}{dV_a} \right]^{-1} \qquad (1)$$

where A is the area of the Schottky barrier diode, e_r is the dielectric constant of the semiconductor, and e_o is the permittivity constant. Thus by changing the reverse bias V_a in small increments, the impurity concentration can be calculated from the slope of the C-V plot. The capacitance is typically measured as the out-of-phase component of a small ac signal superimposed on a large dc bias [1]. The system used to run C-V measurements at WSU Tri-Cities consists of a Princeton Applied Research (PAR) 410 C-V Plotter, an analog-to-digital (ADC) and digital-to-analog (DAC) converter, and an Apple II Plus computer. The Apple computer is used to supply the reverse bias to the DAC which in turn supplies V_a to the PAR 410. The PAR 410 measures and outputs the capacitance of the specimen at each increment of V_a to the ADC which in turn outputs values of C and V to the Apple. A program on the Apple controls all experimental parameters (e.g. , device area, e_r , and conductivity type), data acquisition, and any subsequent data analysis. A typical experiment involved ramping the bias voltage from 0 to 4 V in 10 mV increments and collecting the capacitance values at each discrete point. Plots of C vs. V_a and $1/C^2$ vs. V_a were then constructed using the computer in

order to obtain the depletion width at zero bias (one of the values used in modeling calculations to determine the minority carrier diffusion length) and the majority carrier concentration, respectively.

During the course of this study the Electronic Materials Laboratory at WSU Tri-Cities acquired a Polaron Semiconductor Profiler which can be used to determine the net impurity concentration vs. depth into a semiconductor. The profiler works by placing the specimen in contact with a known area of electrolyte and then applying a bias voltage across the semiconductor/ electrolyte interface. Since this is essentially equivalent to the metal Schottky barrier described in the previous paragraph, data on the majority carrier concentration can be collected by analyzing C-V data from the depletion region. The primary difference results from selecting an electrolyte that can produce a well defined electrochemical dissolution reaction , thus allowing the region of the semiconductor in contact with the electrolyte to be etched at a controlled rate. In this manner the majority carrier concentration can be determined as a function of depth without the increasing bias voltages inherent to a typical C-V measurement. In addition, by utilizing Faraday's Law of electrolysis the depth of etching can be determined from the following equation:

$$W_r = \frac{M}{ZFDA}\int I dt \qquad (2)$$

where W_r is the etch depth, M, Z, and D are the molecular weight, valence, and density of the semiconductor, respectively, F is the Faraday constant, A is the area of the specimen, I is the current drawn, and t is time. Using this relation and changes in dopant concentration between layers, the thickness of the $Al_xGa_{1-x}As$ layer could be determined (layer thickness is one of the parameters used in the modeling calculations to determine diffusion length). Values determined for the majority carrier concentration of AlGaAs films are tabulated in Table 2.

Table 2. Summary of majority carrier measurements.

SPECIMEN	T_g, °C	COMPOSITION	DOPANT; FLOW	DOPANT CONCENTRATION cm^{-3} C-V	POLARON
A0-02-07	720	$Al_{.3}Ga_{.7}As$	DMZn 300 sccm	9.3×10^{16}	—
B0-02-07	720	$Al_{.1}Ga_{.9}As$	SiH_4 40 sccm	2.6×10^{17}	1.9×10^{17}
A0-02-13	720	$Al_{.2}Ga_{.8}As$	SiH_4 40 sccm	5.7×10^{17}	1.8×10^{17}
A0-05-01	720	$Al_{.1}Ga_{.9}As$	DMZn 200 sccm	1.5×10^{17}	—
A0-05-02	720	GaAs	SiH_4 30 sccm	1.7×10^{17}	1.3×10^{17}
A0-05-03	720	$Al_{.1}Ga_{.9}As$	DMZn 120 sccm	1.1×10^{17}	—
A0-05-15	720	$Al_{.1}Ga_{.9}As$	DMZn 120 sccm	8.3×10^{16}	5.5×10^{17}
A0-05-30	780	$Al_{.5}Ga_{.5}As$	DMZn 120 sccm	3.2×10^{16}	1.2×10^{17}
A0-05-31	780	$Al_{.1}Ga_{.9}As$	DMZn 120 sccm	2.2×10^{16}	8.7×10^{16}
A0-06-01	780	$Al_{.2}Ga_{.8}As$	DMZn 120 sccm	2.0×10^{16}	—
B0-06-01	780	$Al_{.2}Ga_{.8}As$	DMZn 120 sccm	6.2×10^{16}	2.2×10^{17}
A0-06-04	780	$Al_{.1}Ga_{.9}As$	DMZn 120 sccm	2.9×10^{16}	—
A0-06-05	780	$Al_{.1}Ga_{.9}As$	DMZn 120 sccm	—	4.3×10^{16}
A0-07-11	780	$Al_{.4}Ga_{.6}As$	DMZn 120 sccm	—	4.4×10^{17}

4. MINORITY CARRIER DIFFUSION LENGTH OF $Al_xGa_{1-x}As$ FILMS

In this section, Schottky barrier fabrication, the approach used for photoresponse measurements, and experimental results for minority carrier diffusion length are discussed.

4.1 Schottky Barrier Photoresponse

If a flux of photons, F, is incident on a Schottky barrier, those photons with $E \geq E_g$ will be able to create electron hole pairs (EHPs). These EHPs can then be collected as an electric current known as the photocurrent (I_{ph}) or short-circuit current (I_{sc}). If the metal layer is thin enough to be partially transparent to light, then some fraction of the incident light can reach the semiconductor and produce a photoresponse (photocurrent). There are three different photoeffects that can take place. First, photons can be absorbed in the metal and excite electrons over the barrier into the semiconductor. Higher energy photons are absorbed completely in the depletion region and the electron-hole pairs are "swept" away by the high electric field (in the depletion region) before they can recombine at interface states resulting in excellent collection efficiency at short wavelengths. Lastly, lower energy photons are absorbed partly within the depletion region and partly within the bulk of the semiconductor creating electron-hole pairs; the minority carrier (whether it be an electron or a hole) created within the bulk must then diffuse to the depletion region edge in order to be collected [2].

The two major contributions to the photoresponse of the Schottky barrier cell come from the depletion region and from the bulk. The collection of current from the depletion region is essentially the same as in a p-n junction device. It is assumed that the high electric field present in the depletion region sweeps carriers out before they can recombine. As a result

$$I_{ph} = I(Depletion\ Region) + I(Bulk) \tag{3}$$

where

$$I(Depletion\ Region) = qTF[1 - \exp(\alpha W)]$$

where $I(Bulk) = qTF\exp(\alpha W)\left[\frac{\alpha L}{1+\alpha L}\right]$ is the transmittance of photons through the metal film, F is the incident photon flux at a specific wavelength of light, α is the absorption coefficient, W is the depletion region width, and L is the minority carrier diffusion length. The reflection of light from the metal surface and absorption in the metal film are accounted for in T.

The collection of current from the bulk of the Schottky barrier cell is essentially the same as from the base of a p-n junction device with a modification due to the less than 100% transmission of light through the metal film. The collection is dependent upon the minority carriers having sufficient lifetime (diffusion length) to diffuse to the depletion region. The above expression for *I(Bulk)* is based on the assumption that the back contact (contact other than the Schottky barrier) is ohmic and if the device thickness is much greater than the minority carrier diffusion length.

The photocurrent can be related to the photoresponse of a Schottky barrier through the relationship

$$I_{ph} = Q_{ext} I_{\max} \tag{4}$$

where $I_{max} = qF$, the maximum possible current assuming each photon incident upon the semiconductor creates an EHP and each EHP is in turn collected as current, and

$$Q_{ext}(External\ Photoresponse) = T\left[1-\exp(\alpha W)+\exp(\alpha W)\left(\frac{\alpha L}{1+\alpha L}\right)\right].$$

Q_{ext}/T provides an excellent measurement of material quality and is termed internal photoresponse (Q_{int}). A summary of this information is provided by Figure 5. In Figure 5a, a photon flux F is incident upon a Schottky barrier device and the short-circuit current (I_{SC}) is being measured. Figure 5b depicts a band diagram of the same device showing electron hole pairs being created within the depletion region width, W, and also outside of the depletion region. Electron hole pairs created within the depletion region are immediately swept out by the high electric field present within the region, but in order for EHPs created outside this region to be collected the minority carriers (holes) must diffuse to the depletion region. Thus, carriers must be

created within the minority carrier diffusion length (L) in order to contribute to the photoresponse.

The presence of a large number of interface states could lead to Fermi level pinning at the surface and would result in a region of effectively "dead" material that would not contribute any EHPs to the device current. The effect of a dead layer can be included in the Schottky barrier model by rewriting the depletion region photocurrent as

$$I(Depl.\ Region) = qT(l)F(l)\{\exp(-\alpha d) - \exp(-\alpha w)\} \quad (5)$$

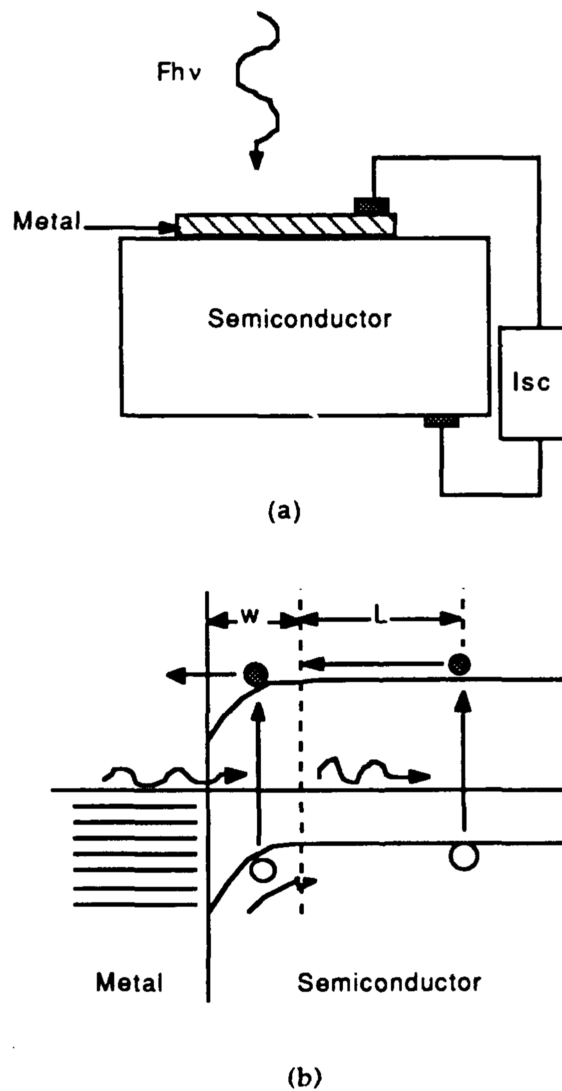

Figure 5. Shown are (a) a Schottky barrier device being measured for I_{SC} with photon flux Fhn, and (b) the associated band diagram. Note that $I_{SC} = Q_{ext} I_{max}$ where $I_{max} = qF$, $Q_{ext} = TQ_{int}$, and $Q_{int} = [(1\text{-}\exp(\text{-}aw) + \exp(\text{-}aw)(aL/1\text{+}aL)]$.

where d is the thickness of the region of dead material. The effect of including a dead layer region in the Schottky barrier model is to decrease the photoresponse of the device in the shorter wavelength (350 to 450 nm) region.

4.2 Fabrication of Schottky Barriers

Schottky barriers were fabricated by vacuum depositing aluminum onto the semiconductor surface. Specimens were prepared for deposition (after being removed from the MOCVD reactor) by rinsing them in deionized (DI) water, rinsing them in methanol, and finally blowing them dry with nitrogen gas. The specimens were then loaded into masks specially designed to produce a Schottky barrier of appropriate size for photoresponse measurements (large enough to allow the entire beam to fall within the device area) and also several Schottky barriers to be used for C-V and DLTS measurements in order to determine majority carrier concentration and the presence of deep level traps, respectively. After the specimens were placed into the masks, they were loaded into the vacuum deposition system along with a quartz witness and the system was pumped down to a typical deposition pressure of 7×10^{-6} torr. In order to achieve acceptably low sheet resistivities and adequate transmittances, the thickness of the aluminum films was limited to values between 70 and 95 Å. Thus, a typical deposition would last five or six seconds (the deposition rate being between 13 and 18 Å/sec). After deposition, the specimens were removed from the vacuum system, and ohmic contacts formed on the front surface of the device by mechanically applying (with teflon coated tweezers) small squares of indium and then alloying them with the semiconductor by applying heat locally. In some cases this simple method would not produce ohmic contacts requiring an additional "burn-in" step that involved passing a current of 0.15 mA (at 35 volts) between two squares of indium placed in close proximity on the semiconductor surface in addition to the previous steps.

4.3 Photoresponse Measurement

After forming the necessary contacts, the specimens were now ready for photoresponse analysis. The photoresponse system consisted of a tungsten filament light source with intensity controlled by a Variac voltage regulator, two separate high-intensity monochromators covering the wavelengths 350

to 700 nm and 710 to 1200 nm, respectively, a light chopper to minimize any possible effects from external sources, and two photomultipliers (one for photoresponse and one for reflectance measurements) that were connected to a power ratiometer. Data acquisition was accomplished through a program run on an Apple II computer that was interfaced to the power ratiometer. Once the data was obtained, it was transferred from the Apple II to a Prime minicomputer to facilitate data reduction and analysis using computer codes previously developed at WSU Tri-Cities.

The external photoresponse is determined by measuring the photocurrent produced by a device for a known incident photon flux (or I_{max}). The internal photoresponse is determined from $Q_{int} = Q_{ext}/T$. T for a given device is calculated from the measured optical constants for the aluminum film deposited on a quartz witness.

In order to determine the optical properties (n and k values) of the Al film, transmittance and reflectance data were taken for the quartz witness. Reflectance data was acquired by placing a non-reflecting piece of black rubber between the quartz witness and the gold-plated hold-down chuck and then following the same procedure for measuring the reflectance as used for the Schottky barrier specimens described previously. Transmittance values were acquired via a two-step process. At each wavelength the value of the reference channel on the power ratiometer was recorded with and without the quartz witness inserted directly in the beam in front of the photomultiplier. The ratio of the two was then determined to be the transmittance of the Al film. In order to obtain the actual reflectance values, data from the ratiometer was entered into a computer analysis program. The n and k of the Al films were determined with a computer-aided analysis that utilizes values of T and R for each photon wavelength and the optical constants of quartz.

After determining the optical properties of the Al film and measuring the photoresponse and reflectance of the Schottky barrier device, a data file was constructed that contained the n and k values of the Al film at each photon wavelength, the n and k values of the $Al_xGa_{1-x}As$ at each photon wavelength, the $Al_xGa_{1-x}As$ layer thickness, the depletion width, the thickness of the dead layer (included only if needed to fit data), the diffusion

length, the diffusivity of the $Al_xGa_{1-x}As$ (a constant), the back surface recombination velocity (assumed to be a constant for these devices), and the bandgap of the semiconductor. The data file was then entered into a modeling program that calculates the external (Q_{ext}) and internal (Q_{int}) photoresponse. The value of diffusion length is then varied until the calculated Q_{int} agrees with the measured Q_{int} at all wavelengths.

4.4 Diffusion Length in $Al_xGa_{1-x}As$ Films

The first specimens to be grown and analyzed were two n-type films with composition $Al_{.1}Ga_{.9}As$ (A0-02-13) and $Al_{.2}Ga_{.8}As$ (B0-02-07) and a p-type film with composition $Al_{.3}Ga_{.7}As$ (A0-02-07). All three films were grown at a temperature of 720 °C (this temperature was chosen because it was the growth temperature in use for actual device structures at the time this study was initiated). Modeling of the photoresponse data revealed that the minority carrier diffusion length of each of these three films was zero as shown in Figures 6, 7, and 8. These results were unexpected since finite diffusion lengths had been measured by a group at Varian [3] for p-type material over the composition range $0.28 \leq x \leq 0.53$. After characterizing these films, emphasis was placed on p-type films with low aluminum content ($x \leq 0.20$) to increase the probability of producing material with a finite diffusion length. With these considerations in mind the next film to be grown, A0-05-01, had composition $x = 0.10$ and p-type conductivity. Modeling of photoresponse data, however, again revealed a minority carrier diffusion length of zero as shown in Figure 9, thus creating some doubt as to the validity of the measurement technique. As a result the approach was applied to n-type GaAs (A0-05-02). A diffusion length of approximately 4.5 μm was determined for the n-type GaAs film by modeling of the photoresponse data shown in Figure 10.

The quality of the fit to the data by the model and the good agreement between the resulting value for the diffusion length and results obtained previously for GaAs homojunction devices restored confidence in the measurement technique and attention was again turned toward p-type AlGaAs of low aluminum content. Specimen A0-05-03 (p-type; $Al_{.1}Ga_{.9}As$) was next in the growth sequence and modeling of the photoresponse data indicated a diffusion length of 0.20 μm as shown by Figure 11, the first

measurement of a finite diffusion length in an AlGaAs specimens grown for this study. All of the AlGaAs specimens discussed thus far were grown directly on GaAs substrates and while it is not likely that this could have been a source of problems in achieving finite minority carrier diffusion lengths in the AlGaAs films, it was decided to study this possibility by growing an epitaxial GaAs buffer layer between the substrate and the AlGaAs. Thus the next film in the series, A0-05-15, was grown under the same conditions as A0-05-03 but with a GaAs buffer layer included in the structure. Modeling of the photoresponse data, as shown in Figure 12, indicated that the diffusion length of this film was zero. The absence of a finite diffusion length in A0-05-15 with the inclusion of a GaAs buffer layer thus served to show that growing the AlGaAs films directly on a GaAs substrate was probably not a limiting factor in the film quality.

For the next film in the series, A0-05-31, it was decided to continue to grow at the higher growth temperature of 780 °C and to also activate an Al-Ga-In eutectic metal bubbler on the arsine source gas line. The reason for activating the bubbler was to try and remove any oxygenated impurities from the arsine source gas prior to reaching the reaction chamber by reacting them with bare Al metal to form Al_2O_3. The removal of these oxygenated impurities has been shown to improve the quality of MOCVD AlGaAs by other researchers as mentioned previously. Photoresponse data were acquired and modeled with the results shown in Figure 13. The diffusion length of approximately 0.40 µm in film A0-05-31 was encouraging because it was the second AlGaAs specimen to exhibit a finite value. However, it had been hoped that the increase in growth temperature and the introduction of the eutectic bubbler would produce a more dramatic impact on the diffusion length. Based upon the results of A0-05-31, it was decided to examine whether or not the increase in T_g along with the introduction of the bubbler would result in finite diffusion lengths for films of higher Al content. Specifically two films of composition $Al_{.2}Ga_{.8}As$, one with a GaAs buffer layer (A0-06-01) and one without (B0-06-01), were grown and analyzed. The photoresponse data and modeling comparisons for these specimens are shown in Figures 14 and 15. Note that the increase in T_g and the inclusion of the eutectic bubbler were not sufficient, at this time, to produce finite diffusion lengths in films with composition $x > 0.10$.

Since the activation of the bubbler had resulted in a finite diffusion length for specimen A0-05-31 ($x = 0.10$) but not for the two specimens with $x = 0.20$, it was decided to grow a series of several $x = 0.10$ films with the bubbler in operation in order to measure the effect of the bubbler on the diffusion length with time. If the bubbler was actually removing oxygenated contaminants from the arsine source gas, then the cleanliness of the arsine line downstream from the bubbler should have improved with each growth run and resulted in higher quality AlGaAs. The next film in the growth series, A0-06-04, had a modeled diffusion length of approximately 0.50 µm as shown in Figure 16. This was an encouraging result since it was the second consecutive $x = 0.10$ film to exhibit a finite diffusion length with the bubbler activated, and the diffusion length improved slightly (from 0.40 to 0.50 µm). The next film, A0-06-05, continued the trend of improved diffusion length in $x = 0.10$ films with the bubbler activated as modeling indicated that $L_e \approx 0.60$ µm as indicated in Figure 17. Results for photoresponse studies of AlGaAs films are summarized in Table 3.

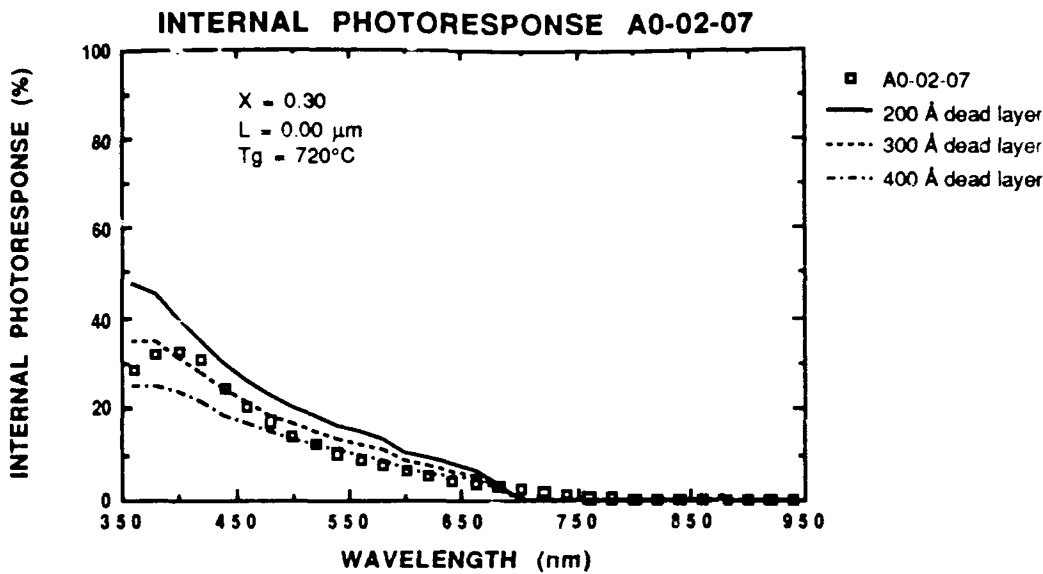

Figure 6. Internal photoresponse versus wavelength for specimen A0-02-07 ($x = 0.30$; p-type). Modeling indicated material of poor quality as $L_e = 0.00$ µm and a dead layer thickness between 300 and 400 Å. Other values used for the modeling calculations were: $H = 4.9$ µm, $W = 0.08$ µm, $D_B = 5.3$ cm^2/sec, $S_{Back} = 1 \times 10^8$ cm/sec, and $E_{Gap} = 1.82$ eV.

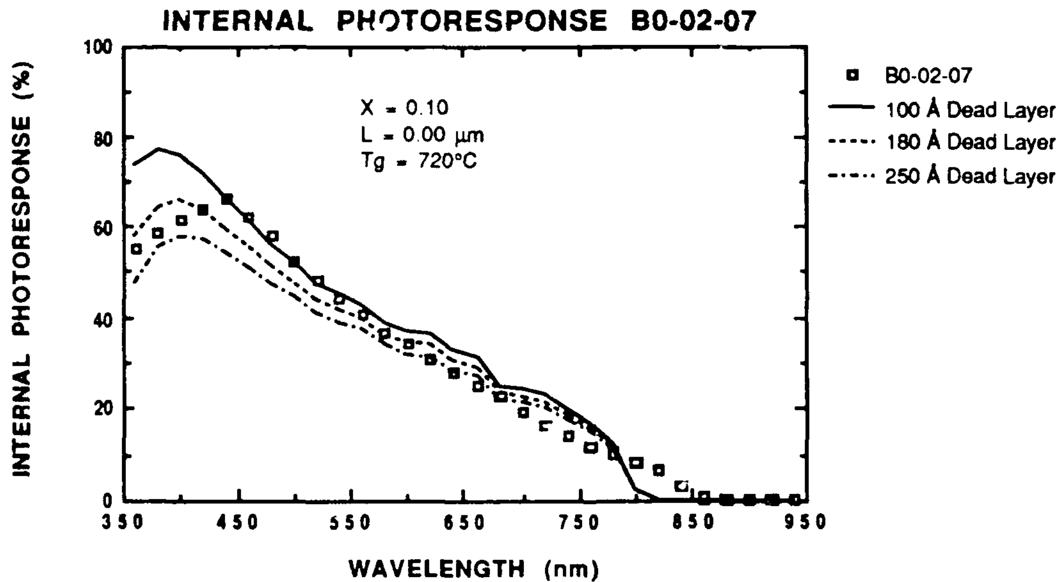

Figure 7. Internal photoresponse versus wavelength for specimen B0-02-07 ($x = 0.10$; n-type). The photoresponse indicated poor material quality as modeling revealed a diffusion length of zero and a dead layer thickness between 180 and 250 µm. Other values used for the modeling calculations were: $H = 3.7$ µm, $W = 0.15$ µm, $D_B = 5.3$ cm^2/sec, $S_{Back} = 1 \times 10^8$ cm/sec, and $E_{Gap} = 1.55$ eV.

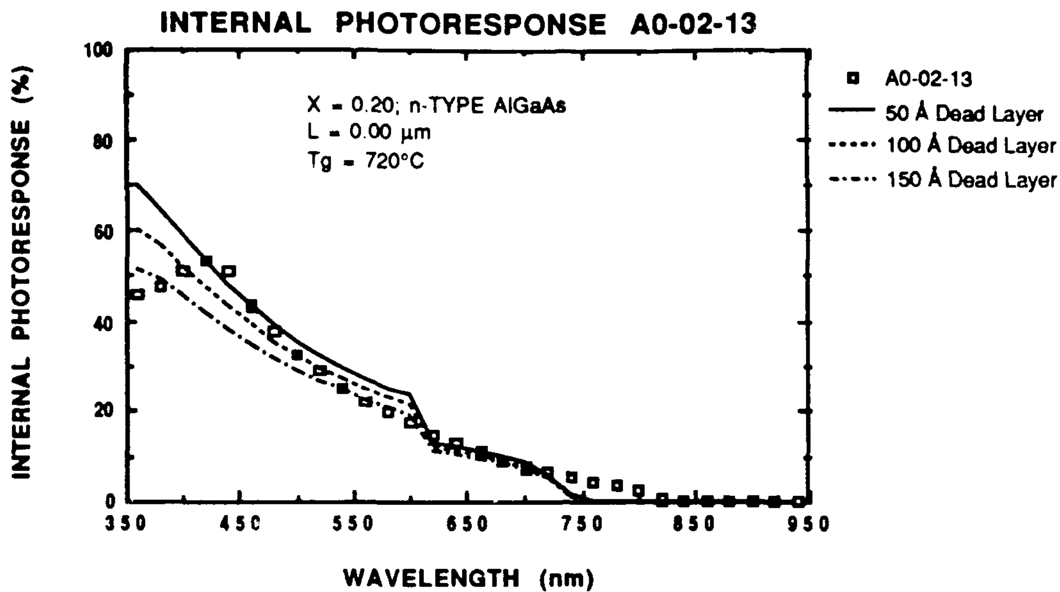

Figure 8. Internal photoresponse versus wavelength for specimen A0-02-13 ($x = 0.20$; n-type). Each ¯ represents an actual data point while the lines represent theoretical fits that utilized the following values: $H = 5.1$ µm, $W = 0.10$ µm, $L_p = 0.00$ µm, $D_B = 5.3$ cm^2/sec, $S_{back} = 1\text{x}10^8$ cm/sec, and $E_{Gap} = 1.69$ eV. The difference in the three lines lies in the thickness of the dead layer as indicated in the plot legend.

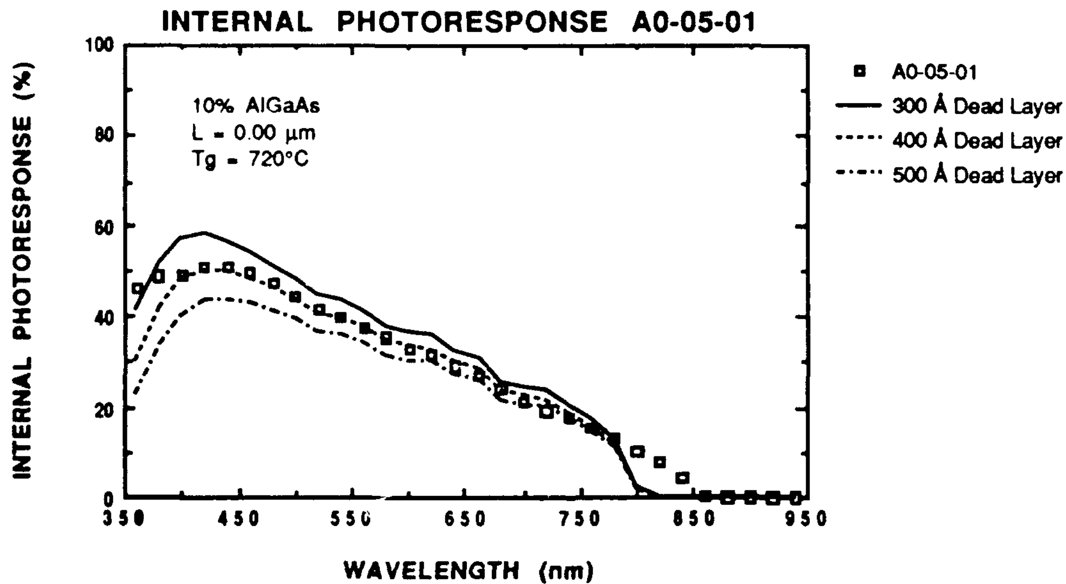

Figure 9. Internal photoresponse versus wavelength for specimen A0-05-01 ($x = 0.10$; p-type). Experimental data are represented by ¯ while the lines represent theoretical fits. Values used for the theoretical fits were: $H = 4.1$ µm, $W = 0.15$ µm, $L_e = 0.00$ µm, $D_B = 5.3$ cm^2/sec, $S_{Back} = 1\text{x}10^8$ cm/sec, and $E_{Gap} = 1.55$ eV. The dead layer thickness is the variable in each fit and the values are included in the plot legend.

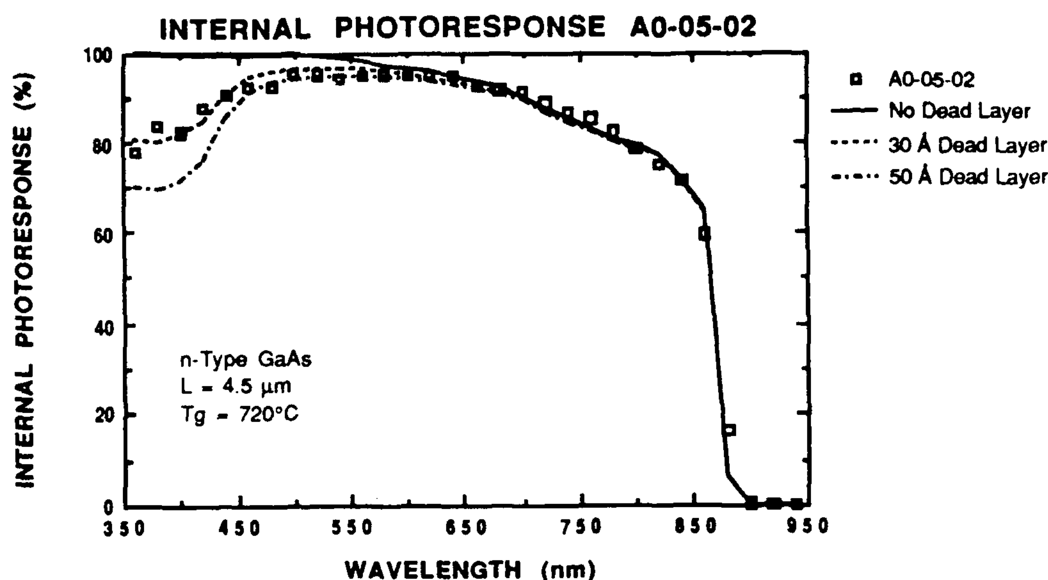

Figure 10. Internal photoresponse versus wavelength for a n-type GaAs specimen (A0-05-02). The experimental data (▫) are modeled closely assuming an L_p of 4.5 µm and a dead layer thickness of 30 Å as indicated. Other values used in the modeling calculations were: $H = 3.2$ µm, $W = 0.20$ µm, $D_B = 5.3$ cm^2/sec, $S_{Back} = 1\text{x}10^8$cm/sec, and $E_{Gap} = 1.42$ eV.

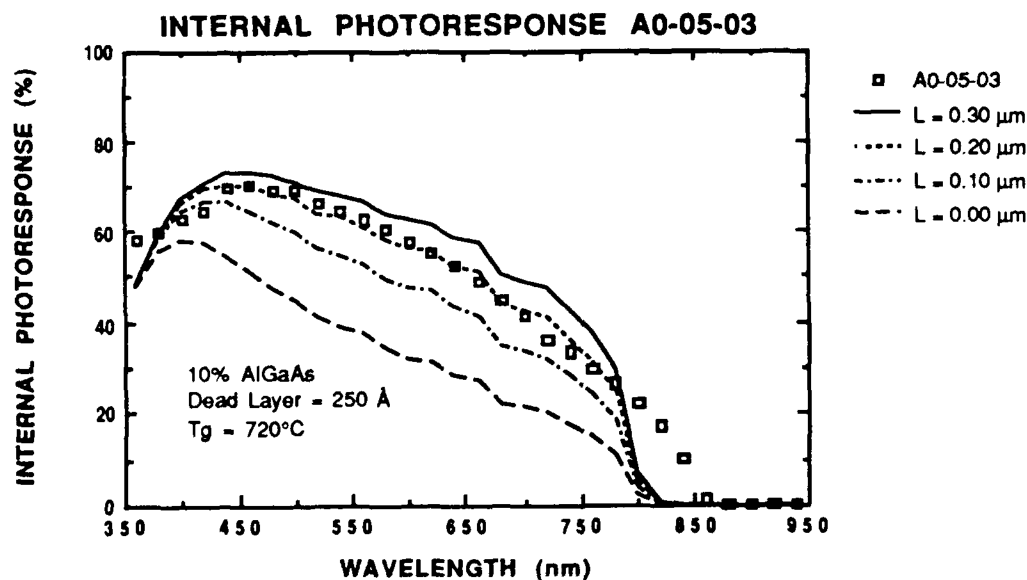

Figure 11. Internal photoresponse versus wavelength for specimen A0-05-03 ($x = 0.10$; p-type), the first AlGaAs layer to exhibit a finite diffusion length. The experimental data are modeled closely assuming an L_e of 0.20 µm and a dead layer thickness of 250 Å. Other values used for the theoretical modeling included; $H = 3.9$ µm, $W = 0.18$ µm, $D_B = 5.3$ cm^2/sec, $S_{Back} = 1\text{x}10^8$ cm/sec, and $E_{Gap} = 1.55$ eV. The difference in the modeled curves is a result of varying L_e as indicated in the plot legend.

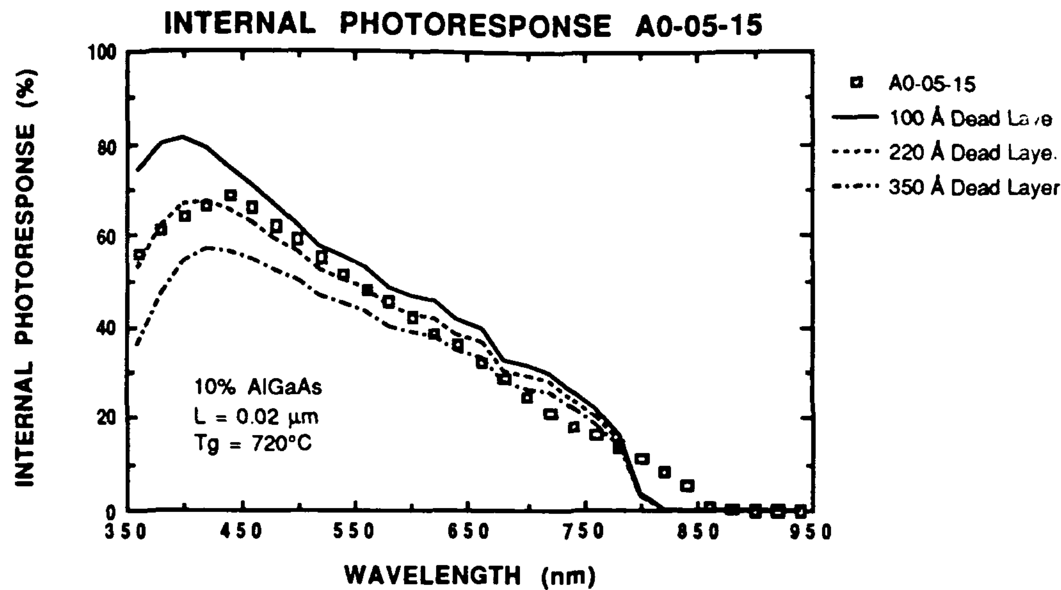

Figure 12. Internal photoresponse versus wavelength for specimen A0-05-15 ($x = 0.10$ µm; p-type). Grown using the same growth parameters as the previous film, it exhibited a near zero diffusion length ($L_e = 0.02$ µm) demonstrating the variability in material quality from run to run. Other values used in the modeling calculations included; $H = 4.3$ µm, $W = 0.20$ µm, $D_B = 5.3$ cm^2/sec, $S_{Back} = 1\text{x}10^8$ cm/sec, and $E_{Gap} = 1.55$ eV. The difference in the modeled curves is due to differing dead layer thicknesses as noted in the plot legend.

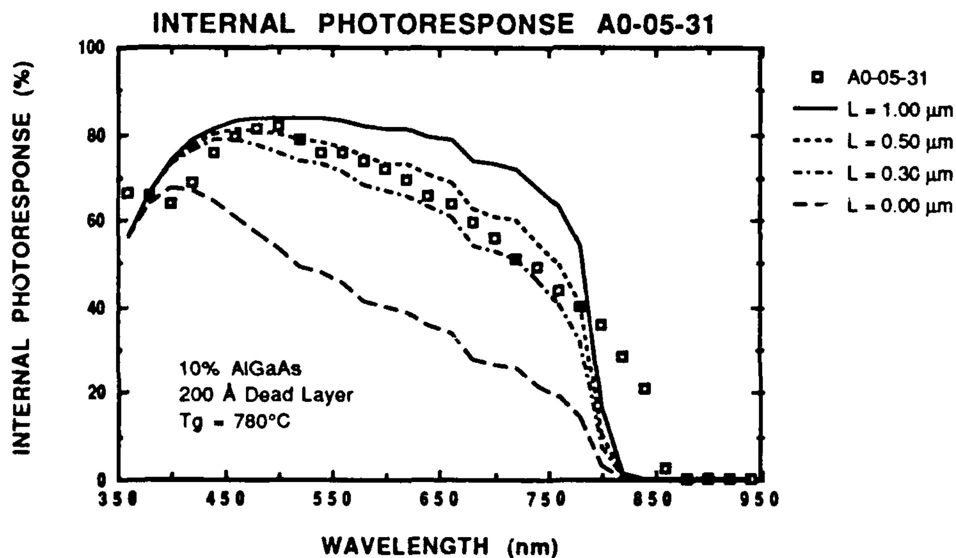

Figure 13. Internal photoresponse versus wavelength for specimen A0-05-31 ($x = 0.10$; p-type), the first AlGaAs layer grown with the eutectic bubbler in operation. Modeling revealed a diffusion length between 0.30 µm and 0.50 µm (assuming a 200 Å dead layer). Other values used in the modeling were: $H = 3.8$ µm, $W = 0.20$ µm, $D_B = 5.3$ cm^2/sec, $S_{Back} = 1\text{x}10^8$ cm/sec, and $E_{Gap} = 1.55$ eV.

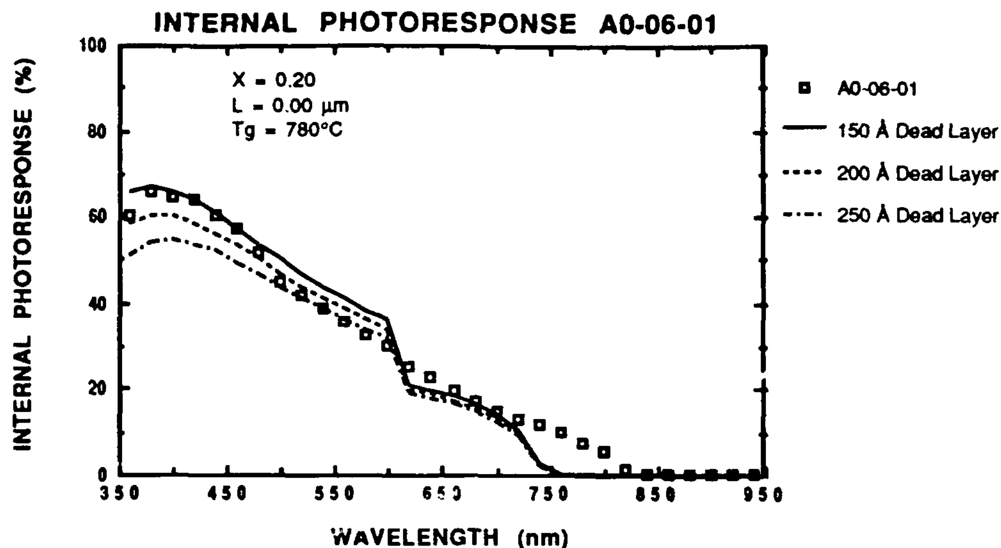

Figure 14. Internal photoresponse versus wavelength for specimen A0-06-01 ($x = 0.20$; p-type). Grown with the eutectic bubbler in operation it was hoped that this would be the first film with $x > 0.10$ to show a finite diffusion length, but this was not the case as modeling indicated $L_e = 0.00$ µm (with a 200 Å dead layer). Other values used in the modeling were: $H = 3.7$ µm, $W = 0.18$ µm, $D_B = 5.3$ cm^2/sec, $S_{Back} = 1\text{x}10^8$ cm/sec, and $E_{Gap} = 1.69$ eV.

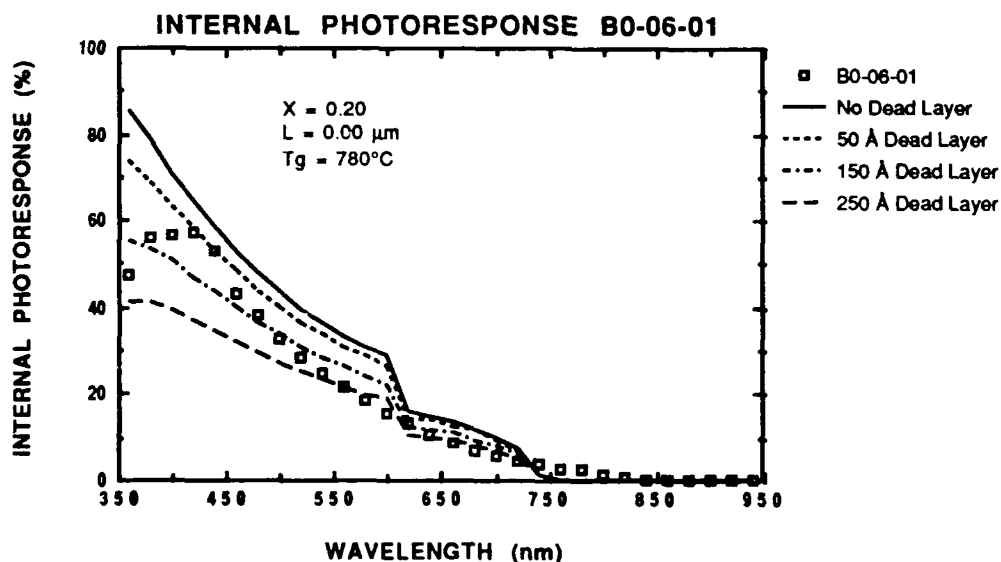

Figure 15. Internal photoresponse versus wavelength for specimen B0-06-01 ($x = 0.20$; p-type). Identical to A0-06-01 with the added addition of a GaAs buffer layer, this film also exhibited a diffusion length of zero. Other values used in the modeling were: $H = 5.6$ µm, $W = 0.12$ µm, $D_B = 5.3$ cm^2/sec, $S_{Back} = 1\text{x}10^8$ cm/sec, and $E_{Gap} = 1.69$ eV.

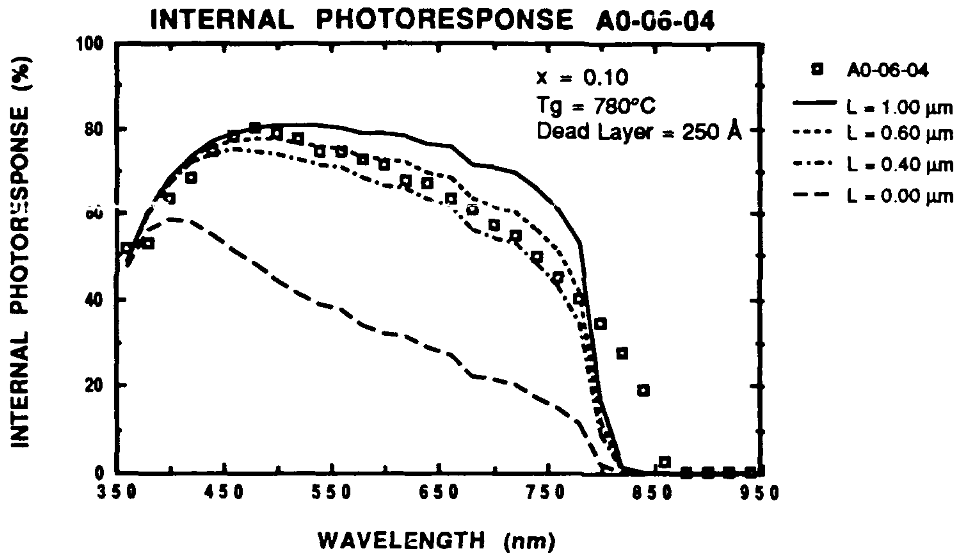

Figure 16. Internal photoresponse versus wavelength for specimen A0-06-04 (x = 0.10; p-type). Of interest is the improvement in L_e from 0.40 µm (A0-05-31) to 0.50 µm (A0-06-04) for material grown using identical growth parameters, indicating that the bubbler was having a positive impact on material quality. Other values used in the modeling calculations were: $H \approx 6.0$ µm, $W = 0.15$ µm, $D_B = 5.3$ cm^2/sec, S_{Back} = 1x10^8 cm/sec, dead layer thickness = 250 Å, and E_{Gap} = 1.55 eV.

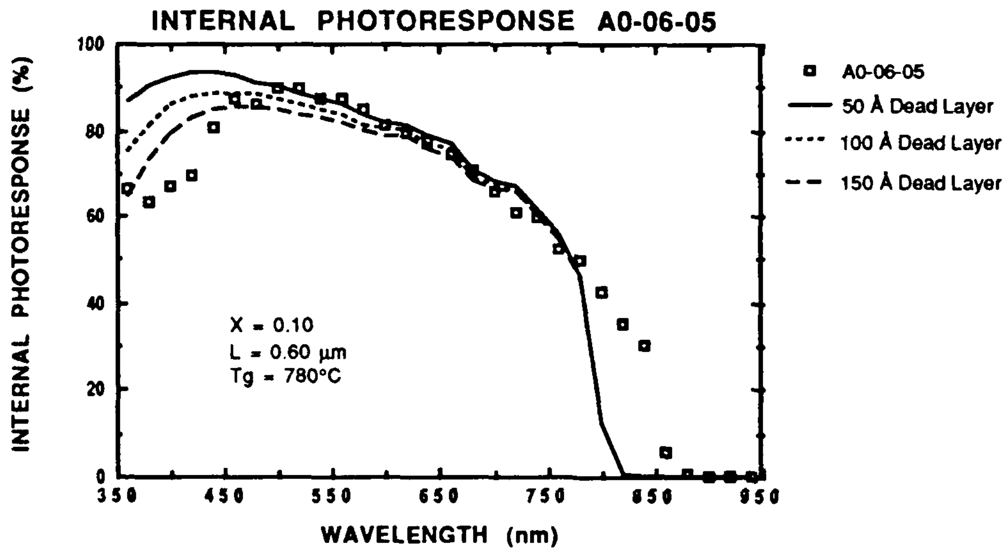

Figure 17. Internal photoresponse versus wavelength for specimen A0-06-05 (x = 0.10; p-type). Note that the diffusion length improved to approximately 0.60 µm indicating that the bubbler was continuing to improve material quality. This specimen exhibited the longest diffusion length of any AlGaAs film grown for this study. Other values used in the modeling calculations were: H = 3.4 µm, W = 0.18 µm, D_B = 5.3 cm^2/sec, S_{Back} = 1x10^8 cm/sec, and E_{Gap} = 1.55 eV. The dead layer thickness was varied as indicated by the plot legend.

Table 3. Summary of photoresponse modeling results.

SPECIMEN	T_g, °C	COMPOSITION AND CONDUCTIVITY TYPE	L, μm	DEAD LAYER, Å	EUTECTIC BUBBLER
A0-02-07	720	$Al_{.3}Ga_{.7}As$ p-type	0.00	≈ 300	No
B0-02-07	720	$Al_{.1}Ga_{.9}As$ n-type	0.00	≈ 200	No
A0-02-13	720	$Al_{.2}Ga_{.8}As$ n-type	0.00	≈ 100	No
A0-05-01	720	$Al_{.1}Ga_{.9}As$ p-type	0.00	≈ 400	No
A0-05-02	720	GaAs n-type	4.50	≈ 30	No
A0-05-03	720	$Al_{.1}Ga_{.9}As$ p-type	0.20	≈ 250	No
A0-05-15	720	$Al_{.1}Ga_{.9}As$ p-type	0.02	≈ 220	No
A0-05-30	780	$Al_{.5}Ga_{.5}As$ p-type	0.00	≈ 300	No
A0-05-31	780	$Al_{.1}Ga_{.9}As$ p-type	0.40	≈ 200	Yes
A0-06-01	780	$Al_{.2}Ga_{.8}As$ p-type	0.00	≈ 200	Yes
B0-06-01	780	$Al_{.2}Ga_{.8}As$ p-type	0.00	≈ 150	Yes
A0-06-04	780	$Al_{.1}Ga_{.9}As$ p-type	0.50	≈ 250	Yes
A0-06-05	780	$Al_{.1}Ga_{.9}As$ p-type	0.60	≈ 100	Yes
A0-07-11	780	$Al_{.4}Ga_{.6}As$ p-type	0.00	≈ 250	Yes

4.5 Discussion of Results for AlGaAs Films

4.5.1 Necessity of Dead Layer in Modeling Calculations

As noted above, it was found necessary to include a "dead layer" region in the modeling calculations to achieve a reasonable fit to the data in the short wavelength (350 to 450 nm) region. The model developed by Hovel assumes that nearly all of the EHPs created in the depletion region are collected due to the high field, as discussed previously. The photoresponse

for the films in this study, especially $Al_xGa_{1-x}As$, tended to fall off in the short wavelength region indicating a need to alter the equation representing the depletion region current in the modeling. The inclusion of a dead layer assumes that the films have a defective surface immediately beneath the Schottky barrier that does not allow EHPs created in the region to be collected. Specifically, it was typically needed to assume the first 150 to 250 Å contributed no EHPs to the photoresponse. A representative diagram of this situation is given by Figure 18. It is interesting to note, however, that the thickness of the dead layer for the n-type GaAs specimen was only 30 Å as indicated in Figure 10 pointing to some difference in the behavior of GaAs and $Al_xGa_{1-x}As$. The presence of the dead layer region may be due the growth procedure itself. After film growth is complete a flow of AsH_3 is maintained in the reaction chamber as the susceptor is cooled down from the growth temperature. Since this flow of AsH_3 may allow As atoms to move into the $Al_xGa_{1-x}As$ lattice without an accompanying Ga atom, Ga vacancies could result. The presence of a high density of Ga vacancies could play a significant role in the formation of a dead layer in these Schottky barrier devices. The dead layer may also be due to procedures leading up to and including the deposition of aluminum to form the Schottky barrier. This is an area that needs to be studied in closer detail.

4.5.2 Evidence Supporting Oxygen Contamination

Initially, a major objective of these studies was to study the diffusion length of n-type $Al_xGa_{1-x}As$ as a function of composition. The initial photoresponse results on low Al content $Al_xGa_{1-x}As$ films indicated material of very poor quality, a somewhat unexpected result based on the results of the study conducted by Ludowise and Dietze [3] where p-type $Al_{0.28}Ga_{0.72}As$ had a modeled diffusion length of ≈ 1.6 μm and even high aluminum content $Al_{0.53}Ga_{0.47}As$ exhibited a finite diffusion length of ≈ 0.2 μm. The poor quality of the first four films, A0-02-07, B0-02-07, A0-02-13, and A0-05-01 indicated that oxygen contamination was a problem in the growth system even though it had been thoroughly leak-checked prior to growth. These initial results would seem to indicate that oxygen contamination was a problem and that the source of contamination was probably one or more of the growth precursors (TMAl, TMGa, or AsH_3).

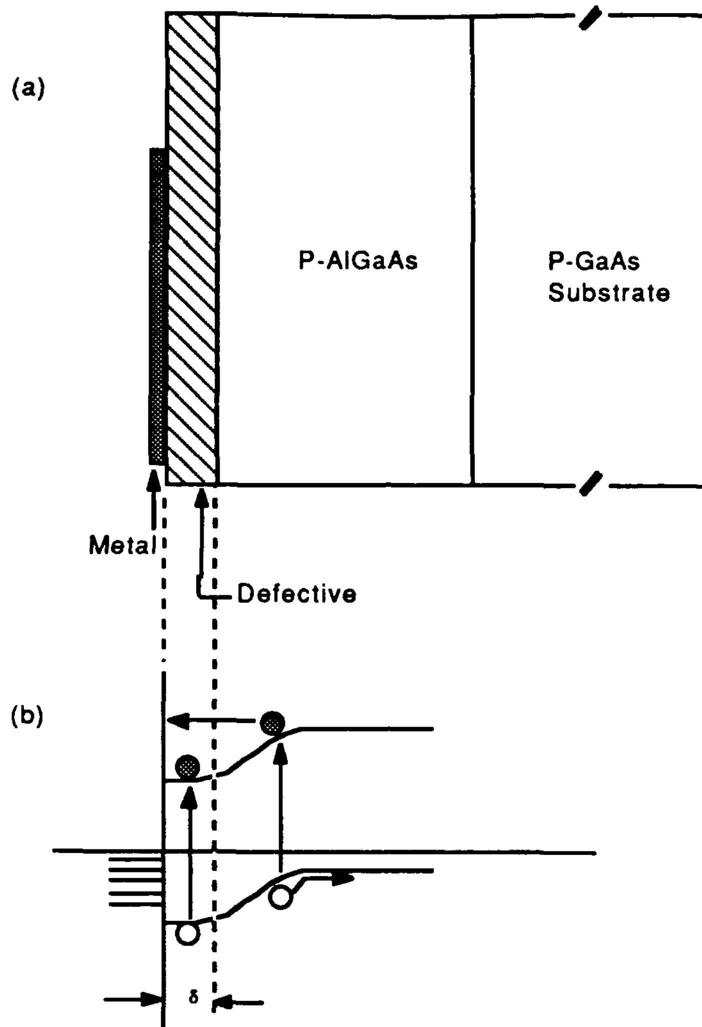

Figure 18. Shown above are (a) the physical representation of the Schottky barrier device including the dead layer, and (b) the corresponding band diagram.

The next result to support the existence of an oxygen contamination problem was the modeled diffusion length of 4.5 µm in n-type GaAs (A0-05-02). This result proved that photoresponse analysis of Schottky barriers was a valid technique to determine the minority carrier diffusion length and it also showed that the WSU Tri-Cities MOCVD reactor was capable of producing high quality semiconductor films. Since it has been shown that the presence of oxygen has no discernible effect on the quality of MOCVD grown GaAs [4, 5], it is not surprising that high quality GaAs was able to be grown. Specifically, the study by Wallis [5] showed that the intentional injection of oxygen into the gas stream had no effect on the concentration of a deep level trap that was always present in the GaAs layers and also that no new deep

traps were created with the intentional injection of O_2. In contrast, even when oxygen was injected in very low concentrations during $Al_xGa_{1-x}As$ growth, a sharp decrease in the net donor density (N_D - N_A) resulted in highly resistive layers, and a deep level trap located at ≈ 0.4 eV below the conduction band (for $x \leq 0.05$) was introduced in high concentrations (>10^{15} cm^{-3}). Similarly, in the study by Tsai [4], an oxygen-related 0.8 eV PL peak did not occur at all in MOCVD grown GaAs, but dominated the PL spectra for $Al_xGa_{1-x}As$ ($x \geq 0.06$) grown under the same conditions. The results of both of these studies indicate that high quality GaAs can be grown in an MOCVD reactor regardless of oxygen contamination, while the quality of $Al_xGa_{1-x}As$ is very dependent on oxygen incorporation.

Many techniques have been employed to improve the quality of MOCVD grown $Al_xGa_{1-x}As$ by reducing the concentration of oxygenated impurities in the film and several have already been discussed in this report (i.e., graphite baffles, eutectic bubbler, and higher growth temperatures). Two of the techniques were used in this experiment, a higher growth temperature and a eutectic bubbler on the AsH_3 source gas line. The next section will examine these two factors more closely and the impact they had on the quality of the $Al_xGa_{1-x}As$ films grown for this study.

5. EFFECT OF EUTECTIC METAL BUBBLER ON $Al_xGa_{1-x}As$ QUALITY

One approach to improving the diffusion length in AlGaAs films consisted of using a eutectic metal bubbler on the arsine line. Results indicate that incorporation of the bubbler had a greater impact on materials quality than the change in growth temperature.

5.1 Operation of Bubbler

The purification of process gases, particularly arsine, using an Al-Ga-In eutectic metal bubbler has been found to significantly improve the quality (as measured by PL) of MOCVD grown AlGaAs [6, 7, 8]. The technique was first described and used by Shealy [9] to remove water vapor and oxygen from hydrogen and nitrogen and then in a following study [8] it was used to remove oxygen and moisture from the arsine source gas used for the MOCVD growth of AlGaAs. They prepared a two-phase solution consisting of the liquid ternary saturated with aluminum and solid aluminum in order to assure the solution remained saturated with aluminum as aluminum was consumed through oxidation. The main advantages associated with using aluminum to getter oxygen are the stability and low vapor pressure of its oxide (Al_2O_3). The use of solid metallic aluminum is not an effective means to getter oxygen due to this inherent stability of the native oxide which protects it against further oxidation. The Al-Ga-In ternary melt is a convenient method of assuring that a continuous supply of bare aluminum metal will be available to react with oxygen and moisture at room temperature. As it is formed, the aluminum oxide floats to the top of the melt.

Once the bubbler is in place, operation is quite simple as it only involves flowing (bubbling) the process gas through the melt at room temperature to allow any water vapor or oxygen present to react with aluminum prior to reaching the reaction chamber. Presently it is generally accepted that the growth of high quality AlGaAs by MOCVD requires the use of gettering on the arsine line (usually in the form of an eutectic bubbler) at a minimum, and may require gettering on every line entering the reaction chamber. The eutectic bubbler incorporated into the MOCVD system used to

grow films for the present study relies on the same basic principle as the one used by Shealy.

5.2 Effect on Minority Carrier Diffusion Length

Initially, films were grown without the eutectic bubbler in operation and it proved to be difficult to grow $Al_xGa_{1-x}As$ films with a finite diffusion length even at the low aluminum content of $x = 0.10$. As a result, only one of the AlGaAs films grown prior to activation of the bubbler, A0-05-03 ($x = 0.10$), exhibited a significant finite diffusion length (0.20 μm). Once the bubbler was activated and included as a part of the growth process, growing AlGaAs films ($x = 0.10$) with a finite diffusion length proved to be an easier task. A finite diffusion length of 0.30 μm was measured for the first film grown with the bubbler in operation, A0-05-31, and the diffusion length increased with each successive growth run producing $x = 0.10$ films. During the course of this study L_e (in $x = 0.10$ material) reached a maximum value of approximately 0.60 μm for film A0-06-05. The internal photoresponse data for all of the 10% films grown for this study are shown in Figure 19. Note the general

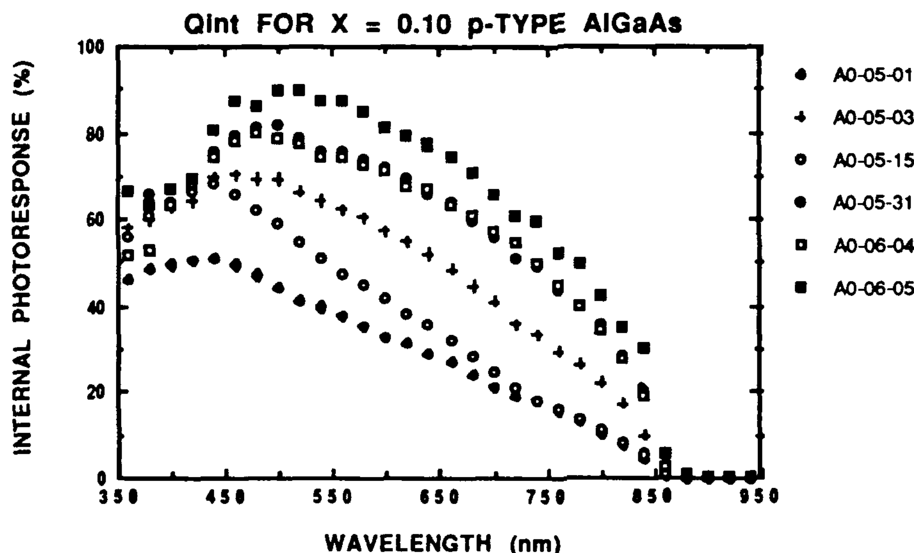

Figure 19. Internal photoresponse versus wavelength for $x = 0.10$ (p-type) specimens. Note the general improvement in photoresponse with time (specimens listed in chronological order with A0-05-01 being grown first and A0-06-05 being last) and, more specifically, the large increase upon introduction of the eutectic metal bubbler (activated for the first time during the growth of specimen A0-05-31).

improvement in response for the last three films (A0-05-31, A0-06-04, and A0-06-05) which were grown with the bubbler in operation. The gradual increase in the diffusion length for the $x = 0.10$ films with the bubbler activated probably indicated that the arsine source gas entering the reaction chamber was becoming increasingly pure (i.e., less oxygenated impurities). It has been mentioned by other authors [3] that the difficulty in obtaining high quality $Al_xGa_{1-x}As$ is due to the extreme sensitivity of the minority carrier diffusion length to trap densities. The density of traps, in turn, depends on the high sensitivity of the MOCVD growth process to background impurities (O_2 and H_2O) in the growth ambient. Thus it could be argued that the bubbler was probably removing one source of oxygenated contaminants from the growth ambient, thereby reducing the total trap concentration and increasing the minority carrier diffusion length.

If oxygen and water vapor in the arsine source gas were the primary contaminants in the AlGaAs films, then the increase in L_e with each successive growth run with the bubbler in operation is to be expected due to the increasing degree of cleanliness of the arsine line downstream from the bubbler. Because there is a finite limit to the cleanliness of the arsine line, it is expected that L_e should reach some peak value and remain on a plateau until the effectiveness of the bubbler starts to diminish due to the consumption of free aluminum from the ternary melt (assuming all other growth conditions remain constant). As the availability of aluminum decreases, the amount of contaminants passing through the bubbler will start to increase and should be reflected by a subsequent decrease in minority carrier diffusion length.

Even with the bubbler in operation, however, it proved to be intractable to grow a film with composition $x > 0.10$ exhibiting a finite diffusion length during the course of the study. The failure to achieve a finite diffusion length for any specimen with composition $x > 0.10$ could have several possible explanations. The improvement in L_e for the $x = 0.10$ films indicates that the purity of the arsine source gas entering the reaction chamber was probably increasing, but it may still have contained oxygenated impurities at levels high enough to be readily incorporated into AlGaAs films of higher aluminum content resulting in oxygen concentrations that were

severely detrimental to material quality. If this was the case, the continued use of the bubbler should further improve the cleanliness of the arsine line downstream from it and hence the arsine source gas arriving at the reaction chamber. Thus, with time it should be expected that the AlGaAs material quality will continue to improve resulting in finite diffusion lengths for material of higher aluminum content. If the continued use of the bubbler does not produce finite diffusion lengths in higher Al content material, it would indicate that there is probably another source of oxygenated contaminants in the MOCVD system.

It could also be argued that the increase in growth temperature from 720 to 780 °C was responsible for the improvement in material quality since it has been demonstrated previously that higher growth temperatures produce higher quality AlGaAs layers [4, 6, 10, 11, 12]. If the growth temperature was the primary factor influencing the minority carrier diffusion length of the AlGaAs films in this study, however, little if any improvement should have been gained with successive growth runs after the temperature was initially increased for film A0-05-31. Because the increased temperature only effects the area in close proximity to the susceptor and does not serve to increase the cleanliness of the reactor, it is believed that its full impact would have been realized on the first growth run and no further improvements would have been gained. Since L_e increased with each successive growth run after A0-05-31 for films of identical composition, it can be concluded that an additional factor besides the increase in T_g was working to improve the $Al_xGa_{1-x}As$ quality. Therefore, while the increase in T_g probably helped to improve material quality, it appears that the bubbler had a more significant impact on the improvement in L_e.

6. GaAs SOLAR CELL GROWTH AND FABRICATION

During the first year of this program, efforts were focused on growth of GaAs and fabrication of GaAs solar cells. Rapid progress was made such that highly efficient cells were fabricated.

6.1 Epi Layer Structure

Epitaxial layer structures as described by Figure 20 were grown with the WSU reactor for GaAs solar cell studies. The as-grown epi-wafer included a GaAs cap layer that provides protection for the 90% AlGaAs window layer, and is used for establishing the front contact as depicted in the figure. After forming contacts to the front surface (bus bar and grid fingers), the remainder of the cap layer is removed except for the region under the contacts. The back AlGaAs reflector layer contains 30% Al.

6.2 P/N Solar Cell Fabrication and Characterization

GaAs P/N solar cells have been fabricated as described by Figure 20 that exhibit AM1 efficiencies greater than 21%. These results are very good, and essentially place the Electronic Materials Group at WSU Tri-Cities at the forefront of GaAs solar cell research. Illuminated current voltage characteristics for one of many cells with an efficiency > 21% are given in Figure 21. Typical results for the internal photoresponse (quantum efficiency) are plotted in Figure 22. Interpretation of the photoresponse data with theory indicates the following minority carrier properties:

L(Emitter)	>	5 μm
L(Base)	>	4 μm
S(Front)	>	10^4 cm/sec
S(Back)	>	10^4 cm/sec

Further improvements can be made in the cell structure and MOCVD growth methods that would lead to efficiencies > 23 %. However, the cell properties reported here represent state-of-art results.

Considerable effort was devoted to interpreting the photoresponse and current voltage characteristics of GaAs cells. Two papers concerning this work are listed in Appendix B.

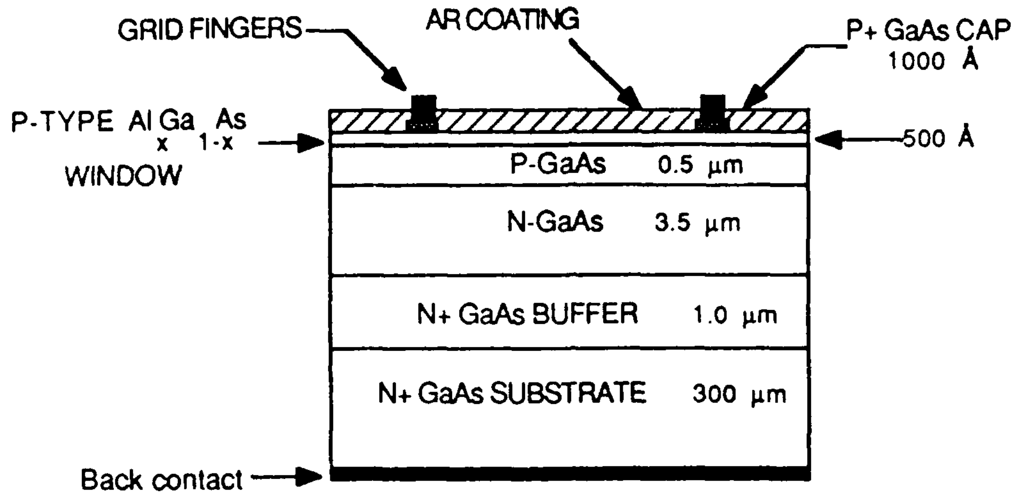

Figure 20. Layered Structure of GaAs Solar Cell Grown and Processed at WSU Tri-Cities.

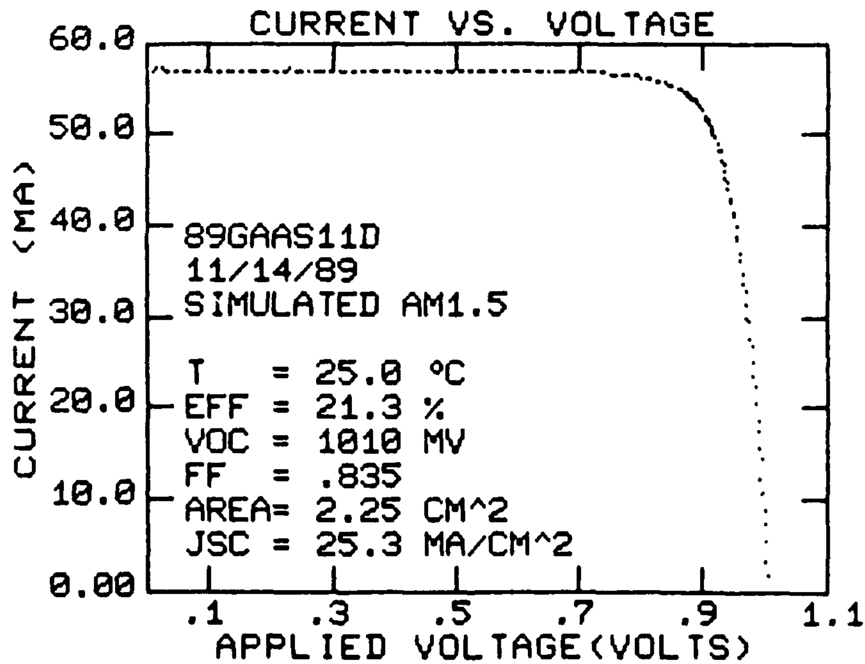

Figure 21. Illuminated I-V Characteristics of WSU Tri-Cities Cell Coupled to Approximate AM1.5 Illumination.

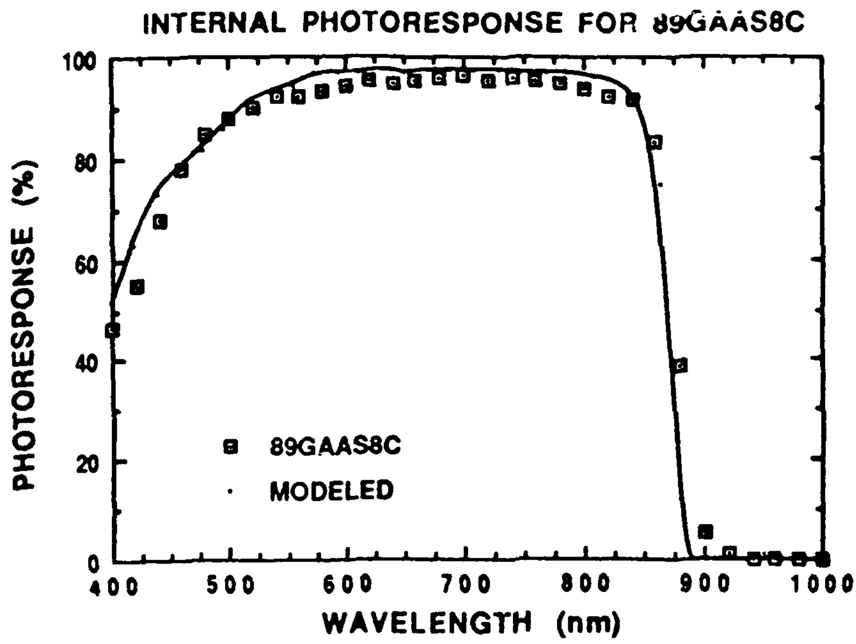

Figure 22. Internal Photoresponse for High Efficiency GaAs Cell.

REFERENCES

1. S. Blight, Solid State Technology, April 1990, 175.
2. H.J. Hovel, *Semiconductors and Semimetals* (Academic, New York, 1975), Vol. II, p. 112.
3. M.J. Ludowise, and W.T. Dietze, J. Appl. Phys. **55**, 4318 (1984).
4. M.J. Tsai, M.M. Tashima, and R.L. Moon, J. Electron. Mater. **13**, 437 (1984).
5. R.H. Wallis, M.a. Forte-Poisson, M. Bonnet, G. Beuchet, and J.P. Duchemin, in*International Symposium on GaAs and Related Compounds*, Vienna, 1980, edited by H.W. Thim (Inst. Phys. Conf. Ser. No. 56, London, 1981), p. 73.
6. T.F. Kuech D.J. Wolford, E. Veuhoff, V. Deline, P.M. Mooney, R. Potemski, and J. Bradley, J. Appl. Phys. **62**, 632 (1987).
7. C.R. Lewis, H.C. Hamaker, and R.T. Green, J. Electron. Mater. **16**, 365 (1987).
8. J.R. Shealy, V.G. Kreismanis, D.K. Wagner, and J. M. Woodall, Appl. Phys. Lett. **42**, 83 (1983).
9. J.R. Shealy, and J.M. Woodall, Appl. Phys. Lett. **41**, 88 (1982).
10. J.P. André, M. Boulou, and A. Micrea-Roussel, J. Cryst. Growth **55**, 192 (1981).
11. S. Takagishi, H. Mori, K. Kimura, K. Kamon, and M. Ishii, J. Cryst. Growth **75**, 545 (1986).
12. K. Tamamura, T Ohhata, H Kawai, and C. Kojima, J. Appl. Phys. **59**, 3549 (1986).

APPENDIX A

Contributors to Program

Dr. Larry C. Olsen	Principal Investigator
	Professor of Materials Science and Engineering
Dr. F. William Addis	Research Associate
Mr. Glen Dunham	Research Associate
Mr. Dan Huber	Ph.D. Student in Materials Science and Engineering
Mr. Mike Maxson	M.S. Student in Materials Science and Engineering
Mr. Dave DeVries	Ph.D. Student in Electrical Engineering

APPENDIX B

Publications

"GaAs Solar Cell Photoresponse Modeling Using PC-1D," presented at the 10th Space Power Research and Technology Conference, Nov. 7, 1989, NASA Lewis Research Center, Cleveland, Ohio. To be published in conference proceedings.

"PC-1D Modeling of Depletion Layer Recombination in GaAs Solar Cells," accepted for presentation at 21st IEEE Photovoltaic Conference, May 21, 1990, Kissimmee, Florida. Will be published in conference proceedings.

APPENDIX C

An MOCVD system can be broken down into four major subsystems: (1) the gas handling system including the growth precursors and carrier gas and also all of the associated plumbing and instrumentation necessary to control gas flows; (2) the reaction chamber and associated heating system in which the pyrolysis reactions and subsequent material deposition occur; (3) the exhaust and/or low-pressure pumping system; and (4) the process control system which controls the entire growth process. Only (1), (2), and (4) will be discussed here. A schematic of the WSU Tri-Cities reactor, a SPI-MO CVD 500XT, is shown in Figure C-1.

1. The Gas Handling System

The gas handling system is designed to deliver precisely controlled amounts of uncontaminated growth precursors to the reaction chamber. This must be accomplished without transients, due to changes in either pressure of flow, that may degrade material quality. The Spire 500XT MOCVD system has four metalorganic (MO) channnels and five hydride channels for transporting the growth precursors. The MO channels consist of a temperature controlled bubbler containing one of the metalorganic sources (such as trimethylgallium) that is fed by a palladium-diffused hydrogen carrier gas and also incorporated is a separate hydrogen boost line to increase reactant transport speed. In addition, the pressure of each bubbler is independently controlled during low-pressure growth. Two of the hydride channels are dedicated to arsine and phosphine, and include eutectic alloy bubblers whose purpose is to remove any trace water and oxygen from the source gas. The remaining three hydride channels are intended for dopants and are equipped with dilution networks allowing controlled flows ranging from 0.05 sccm to 200 sccm. All of the channels are controlled by electronic mass flow controllers, and are injected directly into the vertical barrel reaction chamber by a radial manifold. The valving scheme utilized allows the precursors to be switched from a run (growth) mode to a vent mode. This facilitates a complete purging of the plumbing system prior to injection into the reaction chamber, and allows injection stoppage without having to flush excessive

lengths of plumbing. All critical valves and all of the mass flow controllers are interfaced to the Process Control center noted in Figure C-1.

2. The Reaction Chamber and Heating System

The Spire 500XT has a vertical barrel reactor that is capable of allowing five two-inch or three three-inch wafers to be processed in a single growth run. A ferrofluidic seal transmits rotational motion to the slicon carbide coated susceptor, allowing it to turn at 0-10 rpm. The reaction chamber is constructed of double walled quartz, and in order to minimize any parasitic reactions cooling water is circulated between the walls. Each end of the chamber is sealed by double concentric O-rings and a quadrupole mass spectrometer is used to detect any leaks in the seals. The susceptor (upon which the growth substrate rests) is heated by radiofrequency (rf) induction and can be set to any temperature in the range 200 to 1000° C. The 500XT reaction chamber pressure can be controlled from atmospheric pressure (760 torr) to as low as 76 torr for low-pressure growth.

4. Process Control

An IBM AT computer in conjunction with a Siemens controller, maintains and controls all reactor functions. During an individual growth run over one-thousand separate growth steps are allowed, with each step setting gas flows (to both run and vent), chamber pressure, susceptor temperature and rotation, and length of step. The susceptor temperature, gas flow rate, and chamber pressure can all be ramped linearly or functionally. Two video display terminals are used to monitor the values of all parameters, and these values can also be stored into computer memory. The computer is also assigned the task of monitoring the many safety interlocks built into the 500XT and can warn the reactor operator if a questionable situation arises or automatically shut the reactor down into a safe mode if the condition warrants such action. The emergency shutdown does not require house electricity, and thus can proceed even in the event of a complete power failure.

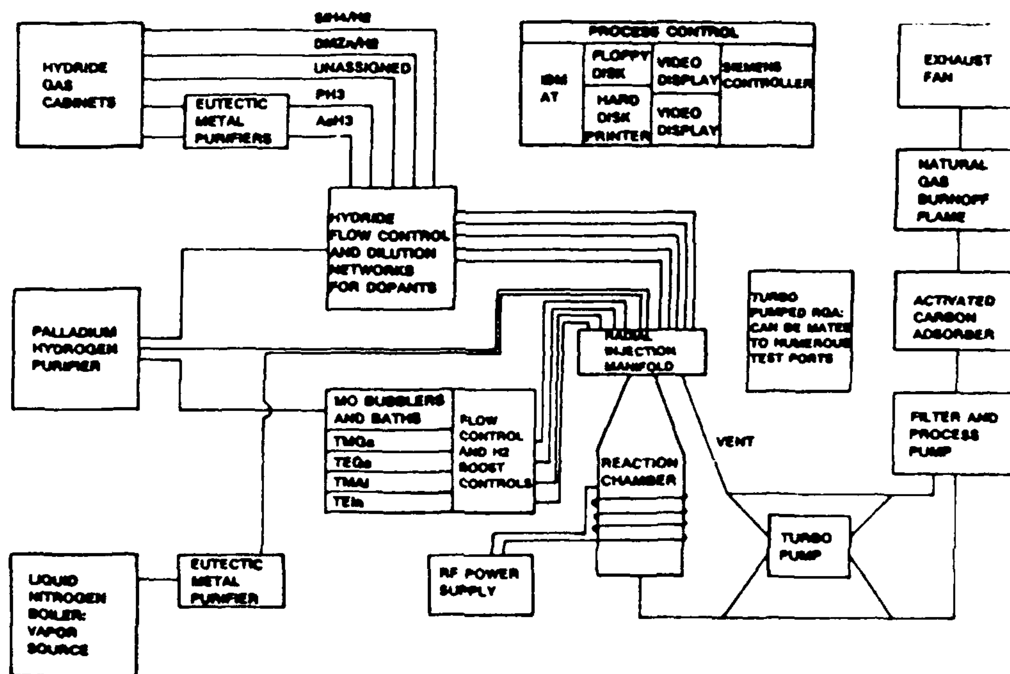

Figure C-1. Spire 500XT MOCVD System Installed in the Electronic Materials Laboratory, WSU Tri-Cities.